Bulletin of Volcanology (2020) 82: 24
https://doi.org/10.1007/s00445-019-1350-5

RESEARCH ARTICLE

Did ice-charging generate volcanic lightning during the 2016–2017 eruption of Bogoslof volcano, Alaska?

Alexa R. Van Eaton[1] · David J. Schneider[2] · Cassandra M. Smith[2,3] · Matthew M. Haney[2] · John J. Lyons[2] · Ryan Said[4] · David Fee[5] · Robert H. Holzworth[6] · Larry G. Mastin[1]

Received: 30 June 2019 / Accepted: 12 December 2019 / Published online: 6 February 2020
© This is a U.S. government work and not under copyright protection in the U.S.; foreign copyright protection may apply 2020

Abstract

The 2016–2017 shallow submarine eruption of Bogoslof volcano in Alaska injected plumes of ash and seawater to maximum heights of ~ 12 km. More than 4550 volcanic lightning strokes were detected by the World Wide Lightning Location Network (WWLLN) and Vaisala's Global Lightning Dataset (GLD360) over 9 months. Lightning assisted monitoring efforts by confirming ash-producing explosions in near-real time, but only 32 out of the 70 explosive events produced detectable lightning. What led to electrical activity within some of the volcanic plumes, but not others? And why did the lightning intensity wax and wane over the lifetime of individual explosions? We address these questions using multiparametric observations from ground-based lightning sensors, satellite imagery, photographs, acoustic signals, and 1D plume modeling. Detailed time-series of monitoring data show that the plumes did not produce detectable lightning until they rose higher than the atmospheric freezing level (approximated by − 20 °C temperatures). For example, on 28 May 2017 (event 40), the delayed onset of lightning coincides with modeled ice formation in upper levels of the plume. Model results suggest that microphysical conditions inside the plume rivaled those of severe thunderstorms, with liquid water contents > 5 g m^{-3} and vigorous updrafts > 40 m s^{-1} in the mixed-phase region where liquid water and ice coexist. Based on these findings, we infer that 'thunderstorm-style' collisional ice-charging catalyzed the volcanic lightning. However, charge mechanisms likely operated on a continuum, with silicate collisions dominating electrification in the near-vent region, and ice charging taking over in the upper-level plumes. A key implication of this study is that lightning during the Bogoslof eruption provided a reliable indicator of sustained, ash-rich plumes (and associated hazards) above the atmospheric freezing level.

Keywords Volcanic lightning · Volcanic ash · Surtseyan · Phreatomagmatic · Magma-water interaction

This paper constitutes part of a topical collection:

The 2016-17 shallow submarine eruption of Bogoslof volcano, Alaska

Editorial responsibility: K. Wallace; Special Issue Editor N. Fournier

Electronic supplementary material The online version of this article (https://doi.org/10.1007/s00445-019-1350-5) contains supplementary material, which is available to authorized users.

✉ Alexa R. Van Eaton
avaneaton@usgs.gov

[1] U.S. Geological Survey, Cascades Volcano Observatory, Vancouver, WA, USA

[2] U.S. Geological Survey, Alaska Volcano Observatory, Anchorage, AK, USA

[3] University of South Florida, School of Geosciences, Tampa, FL, USA

[4] Vaisala, Inc., Boulder Operations, Louisville, CO, USA

[5] Alaska Volcano Observatory, Geophysical Institute, University of Alaska Fairbanks, Fairbanks, AK, USA

[6] Department of Earth and Space Sciences, University of Washington, Seattle, WA, USA

Introduction

December 2016 marked the beginning of the shallow submarine eruption of Bogoslof, an island volcano partly submerged beneath Alaska's Bering Sea (Fig. 1a). Most of the explosive events originated under shallow seawater (depths 5–100 m), but dramatic reshaping of the vent led to shifts between submarine and subaerial activity over the 9-month eruption (Coombs et al. 2019; Waythomas et al. 2020). Seventy discrete explosions were punctuated by time breaks, sending plumes of ash and vaporized seawater up to ~12 km above sea level (asl). Roughly half of these events produced detectable lightning. The electrical activity aided monitoring efforts by verifying the presence of hazardous airborne ash (Coombs et al. 2018). It also provided a means to study electrification of volcanic plumes from the shallow submarine realm.

The origin of lightning in volcanic eruptions remains a topic of great interest to the research community. In some respects, the process is straightforward. First, airborne particles undergo electrifying collisions. Then, circulation within the plume carries charged particles into separate regions, building up an electric field that triggers lightning (Mather and Harrison 2006; James et al. 2008). Generally, the taller, more powerful eruption plumes tend to produce more abundant, energetic lightning (McNutt and Williams 2010). But the details of exactly how and where electrical discharges originate—in the volcanic vent, upper atmosphere, or some combination—are central to the question of how to use lightning data to identify the timing and severity of volcanic hazards. These aspects have come under scrutiny with new observations from active eruptions and laboratory experiments.

Several studies over the past decade have suggested that *ice charging* plays an important role in the generation of globally-detectable volcanic lightning (Williams and McNutt 2005; Thomas et al. 2010; Arason et al. 2011). In ordinary thunderstorms, the presence of ice is not only important, but essential, for lightning to occur (Saunders 2008). The same has been inferred for convective wildfire plumes (LaRoche and Lang 2017). These systems produce lightning when there is a vertical flux through the mixed-phase region of the cloud, prompting collisions of ice crystals, soft hail (graupel), and supercooled liquid drops (Tsutomu 1978; Saunders and Peck 1998; Deierling et al. 2008; Emersic and Saunders 2010). Observations and numerical simulations show that ice and hailstones can readily develop in eruption columns, especially if magma-water interaction takes place, and the plume rises into freezing upper levels of the atmosphere (Van Eaton et al. 2012; Van Eaton et al. 2015).

Yet, there are also examples of *silicate charging* in nature—electrified sand storms and dust devils, for example (Williams et al. 2009). Silicate charging involves (1) fractoemission from fracturing rock (James et al. 2000; James et al. 2008) and (2) tribocharging from colliding ash particles (Cimarelli et al. 2013; Méndez Harper and Dufek 2016; Gaudin and Cimarelli 2019). Recent field campaigns have emphasized that silicate charging provides the sole source of electrification in smaller plumes that do not rise high enough to freeze. For example, eruptions of Sakurajima Volcano in Japan have produced lightning within seconds of explosive onset, with plume heights < 1 km above the vent and plume temperatures hotter than 100 °C (Cimarelli et al. 2016; Behnke et al. 2018; Smith et al. 2018b). But when it comes to larger eruptions capable of producing ice and other hydrometeors, it is currently unknown how the relative roles of silicate- and ice-charging regulate lightning development over the lifecycle of a volcanic plume.

The gold standard in lightning studies involves deploying a lightning mapping array, or LMA, close to a volcano (within 10 s of km) to measure the very high frequency radiation produced by electrical discharges. Studies using this approach have identified three broad categories of electrical signals from volcanic eruptions (Thomas et al. 2010; Behnke et al. 2013). First,

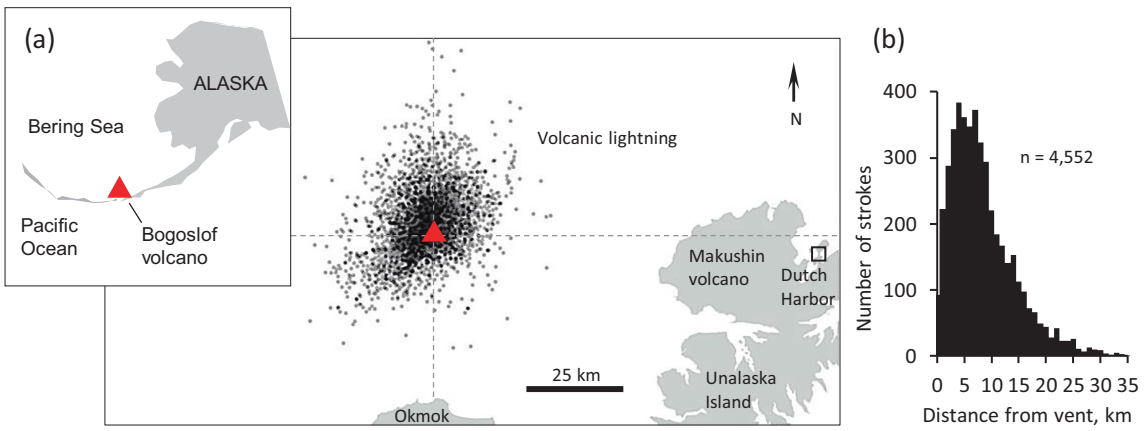

Fig. 1 Area map of Bogoslof volcano (**a**) in Alaska's Aleutian arc and locations of volcanic lightning detected by the combined WWLLN and GLD360 dataset from December 2016 to August 2017. **b** Histogram of lightning locations ($n = 4552$ strokes) shows that most of the electrical activity occurred within 25 km of the Bogoslof, assuming a vent location of 53.9334 N, 168.0392 W

continual radio frequency impulses (also known as *vent discharges*) can be detected before the ash plume even rises above the crater rim (Behnke et al. 2018). This radiation source is not technically lightning at all, but a type of 'cold' plasma discharge confined to the high-velocity jet (Behnke et al. 2018). Continual radio frequency impulses are a unique signature of a volcanic eruption—they have not yet been detected from any other type of thunderstorms. Furthermore, they seem to preferentially occur during impulsive, ash-rich explosions (Smith et al. 2018b). The second type of electrical discharge is *near-vent lightning*, which develops some seconds to minutes after eruptive onset. These relatively small-scale discharges occur within a few kilometers of the volcanic vent, characterized by flash lengths < 7 km (based on the 2006 eruption of Augustine in Alaska). The third category, *plume lightning*, develops after the eruption column has become convective. The flashes exceed ~ 7 km in length and may take place far from the vent, within the vertical column, umbrella cloud, and downwind ash plume. For example, the 2015 eruption of Calbuco in Chile generated volcanic lightning > 100 km downwind (Van Eaton et al. 2016). Plume lightning is indistinguishable from ordinary thunderstorm lightning in terms of electrical characteristics (Thomas et al. 2010; Behnke et al. 2013). However, it is not clear whether silicate charging, ice charging, or some combination is required to produce high rates of globally detectable lightning in volcanic plumes. Is ice a necessary ingredient, as in regular thunderstorms and wildfires?

The Bogoslof eruption provides an unusual opportunity to investigate this question. The explosions were generally discrete and well-defined, with time breaks on the order of hours to weeks. Plume heights were moderate, mostly in the range of 4–10 km asl (maximum 12 km), and atmospheric conditions were quantified using weather models (ERA-interim reanalysis) (Schneider et al. 2020; Schwaiger et al. 2020). Satellite analysis shows that the eruption clouds were rich in condensed water and ice (Lopez et al. 2020; Schneider et al. 2020). Furthermore, the eruptive infrasound took on a different character depending on the presence (or absence) of seawater flooding the volcanic vent (Fee et al. 2020). This multiparametric time series allows us to investigate the lightning during different stages of eruption development and seawater interaction. First, we cover some relevant background on the eruption dynamics and detection methods. Then, we examine the overall lightning characteristics, and unpack the details of eight well-characterized, intensely electrified explosions. Our overall aims are to shed light on the origin of the volcanic lightning, and better understand its operational niche during eruption response.

The 2016–2017 Surtseyan eruption of Bogoslof

Bogoslof volcano is located in the central Aleutian arc of Alaska (Fig. 1). Although the majority of the stratovolcano is submerged beneath the Bering Sea, its summit rises 100–150 m above the water's surface and forms Bogoslof Island, a protected wilderness area and important breeding site for seabirds, seals, and sea lions. In December 2016, Bogoslof erupted for the first time since 1992. The activity consisted of 70 recorded explosive events and at least two phases of subaerial dome growth, all primarily basaltic in composition (Loewen et al. 2019). Most of the explosions were short-lived and pulsatory on timescales of minutes to tens of minutes, with only a few sustained for more than an hour (Wech et al. 2018; Lyons et al. 2020). The volcanic plume heights generally remained within the troposphere, although some rose to modestly stratospheric levels (note: the cold-point tropopause ranged 7–13 km high during the eruption). Airborne ash disrupted local and international air traffic for months, and on three occasions, ash was deposited on communities or ships downwind (Coombs et al. 2018; Coombs et al. 2019). From satellite, nearly all the volcanic clouds appeared light in color and lacked a brightness temperature difference in multispectral imagery, suggesting that the ash signal was masked by abundant water. Schneider et al. (2020) concluded that the high-altitude clouds detected by satellite were ashy and phreatomagmatic—not merely ash-free clouds of steam—based on (1) deposition of juvenile ash every time the clouds drifted over land or ship; (2) measurable growth of Bogoslof Island from high-temperature pyroclastic ejecta; and (3) abundance of magmatic SO_2 gas produced by the explosions, as detected by Lopez et al. (2020). In other words, the plumes were water-rich, but not ash poor.

Seawater flooded freely into the crater during most of the eruption, but buildup of lava domes and tephra periodically blocked access, leading to phases of subaerial activity (Coombs et al. 2019; Waythomas et al. 2020). These changes could be tracked using infrasound data because the acoustic signals took on a different character when the eruption plumes were blasting up through seawater versus directly into the air. When the acoustic source originated underwater, the higher-frequency infrasound was muffled, and only the lower frequencies (< 2 Hz) reached the microphone array on Okmok volcano ~ 60 km away (Fee et al. 2020). In contrast, eruptions directly into air retained the higher-frequency infrasound. This technique made it possible to identify when there was water infilling the vent, and likely, enhanced magma-water interaction during individual eruptive events.

The Bogoslof eruption was similar in several respects to the 1963–1967 Icelandic eruption of Surtsey, the type-example of *Surtseyan* volcanism (Thorarinsson 1967; Walker and Croasdale 1972; Moore 1985; Houghton et al. 2015). Bogoslof and Surtsey both saw prolonged interaction of magma and seawater, generating phreatomagmatic plumes rich in volcanic lightning, but generally < 15 km high (Fig. 2b). They were both small-volume, basaltic, and shallow submarine-to-emergent in nature. Bogoslof's pyroclast textures are

consistent with slowly-ascending, chilled magma (Loewen et al. 2019; Lyons et al. 2019). But it remains to be seen if this is quantitatively different from Surtsey's eruptive products in terms of bubble textures and crystal content (c.f., Schipper and White 2016).

In the mid-1960s, there was an ambitious field campaign to measure Surtsey's electrical signals (Anderson et al. 1965). Focusing on a period of activity from 5 to 16 February 1964, Anderson et al. (1965) flew an airplane directly through the clouds with electric field meters embedded in the wing tips. On one of these airborne surveys, the crew noted volcanic bombs shooting up past the aircraft at 500 m altitude. Next, they equipped a fishing vessel with instruments to measure electrical potential, sailing within 100 m of the active crater and weaving underneath the ash clouds. The team also spent time taking direct observations with long-exposure photography and hand-drawn sketches of volcanic lightning from the nearby village of Vestmannaeyjar. Several findings are worth highlighting. Over their period of observation, Surtsey's lightning (1) occurred within seconds of explosive onset, (2) was confined within the lower regions of the plumes, and (3) developed exclusively from high-velocity jets of black tephra, yet was absent from the ash-poor steam explosions. Although one steam plume from a lava-ocean entry on 24 July 1964 did carry a net positive charge, it failed to generate visible lightning. Overall, these observations are consistent with what would now be recognized as *near-vent lightning*—which has been linked to silicate charging within the conduit and jet (Smith et al. 2018b). Notably, Anderson et al. (1965) discerned that the electrical activity in December 1964, which was before the instruments were deployed (pictured in Fig. 2b), produced a different style of visually "more intense electrical displays," which they suggested may have been related to thunderstorm electrification processes (i.e., ice charging).

Compared to Surtsey, direct visual observations of the Bogoslof eruptions were scarce. Figure 2d shows the only photograph of volcanic lightning captured during the entire eruption. The closest populated area is the city of Unalaska (~4.5 k residents), hosting the port of Dutch Harbor about 100 km east of Bogoslof. Although a Federal Aviation Administration webcam was pointed toward the volcano, poor visibility prevented consistent observations. Therefore, our plume heights are determined exclusively from satellite (Lopez et al. 2020; Schneider et al. 2020). Without any sensors directly on the island, and no weather radar within range, the 70 explosive events were defined by remote monitoring

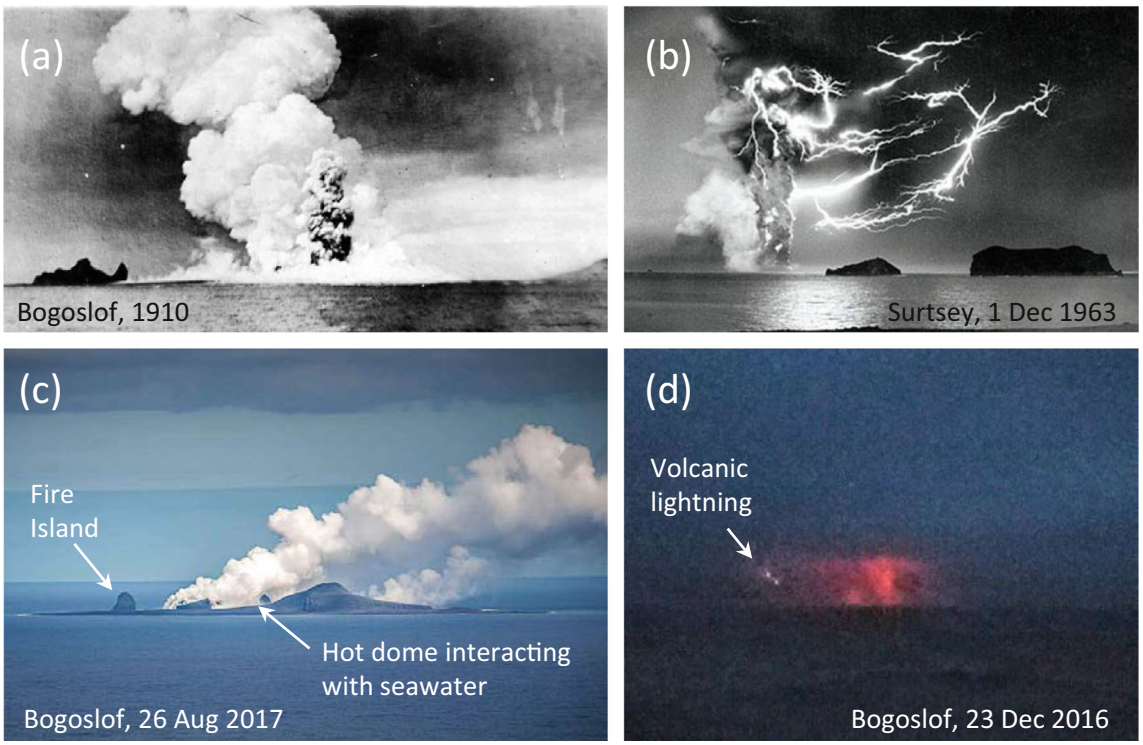

Fig. 2 Photographs of phreatomagmatic activity from Bogoslof in Alaska and Surtsey in Iceland. **a** Water-rich tephra explosion from Bogoslof on 18 September 1910, taken by F.E. Bagger; http://vilda.alaska.edu/u?/cdmg2,3102. **b** Long-exposure (90-s) nighttime photograph of volcanic lightning from the Icelandic eruption of Surtsey on 1 December 1963, when the plume was ~ 8 km asl, by Sigurgeir Jónasson (Jónasson 1965). **c** Steam-dominated plume from Bogoslof on 26 August 2017 due to interaction of seawater and a fresh lava dome (not categorized as an explosive event). Taken from an aircraft about 24 km SW, by Dave Withrow (NOAA). No lightning was detected from this ash-poor plume. **d** The only photograph of volcanic lightning from the 2016–2017 eruption of Bogoslof was captured in the early morning of 23 December 2016 by US Coast Guard crew. Image shows lightning and a towering, incandescent column rising up into the regional cloud deck; AVO image ID 103591

data, including infrasound, seismicity, satellite-detected ash clouds, and ground-based radio antennas to detect volcanic lightning (Coombs et al. 2018; Coombs et al. 2019). The eruption was geophysically monitored in unprecedented detail for a submarine volcano (Tepp et al. 2020). Using this dataset, we address why some of the explosions produced more lightning than others—and some, not at all. We aim to build on the landmark observations of electrical activity from Surtseyan eruptions (Anderson et al. 1965), optimize the use of lightning in volcano monitoring (Behnke and McNutt 2014), and develop a more quantitative understanding of what globally-detected lightning tells us about eruption hazards in near-real time (Shevtsov et al. 2016; Van Eaton et al. 2016; Coombs et al. 2018).

Data, terminology, and methods

Several lightning networks and novel detection methods were brought to bear on Bogoslof's electrical activity during the December 2016–August 2017 eruption. We use measurements from the following sources:

- The World Wide Lightning Location Network's Global Volcanic Lightning Monitor (WWLLN)
- Vaisala's Global Lightning Dataset (GLD360)
- Two-sensor solutions from GLD360 (using 2 sensors instead of the standard 3+)
- Volcanic thunder detected by the microphone array on Okmok volcano, 60 km south of Bogoslof, as reported by Haney et al. (2018) and Haney et al. (2020)
- Lightning detected as *glitches* on the microphone array cables at Okmok volcano (Haney et al. 2020)

Not included in this study are detections from two additional Earth Networks Total Lightning Network stations, which were deployed in the Aleutians toward the end of the eruption. Data from those sensors will be examined in follow-up work (Lapierre et al. 2018; Haney et al. 2020). No LMA was installed during the eruption (c.f., Behnke et al. 2013; Behnke et al. 2014), so our measurements do not capture all of the electrical discharges that occurred. It is also worth noting that the eruptive activity was outside the coverage of satellite-based, geostationary lightning mappers (Schultz et al. 2016; Andrews et al. 2018).

For this paper, we use the term *strokes* to broadly encompass the individual lightning detections regardless of detection method or classification as in-cloud or cloud-to-ground. In practice, a single flash of lightning can generate multiple strokes, but we have not grouped the strokes into parent flashes. Return strokes (and cloud pulses) create radio waves in the very low frequency (VLF) band from 3 to 30 kHz. The VLF energy from lightning propagates thousands of kilometers away at the speed of light, conducted by the Earth-ionosphere waveguide. Long-range detection systems like WWLLN and GLD360 use ground-based radio antennas to measure the electric or magnetic field, providing 2D lightning locations with a spatial accuracy typically < 5 km and a timing accuracy on the order of 10 μs (Abarca et al. 2010; Said et al. 2013). Altitudes of lightning sources were not directly measurable with the network configurations available during our study.

WWLLN had approximately 80 active sensors worldwide at the time of the eruption. The detection algorithm uses five or more stations to locate VLF radiation using the time of group arrival to each sensor (Rodger et al. 2005). Previous studies of relative detection efficiency have shown that WWLLN locates about 10% of all lightning detected by VLF sensors around the world (Hutchins et al. 2012a; Bitzer and Burchfield 2016). The network is particularly sensitive to cloud-to-ground lightning, capturing 40–50% of all strokes with peak current > 40 kA (Hutchins et al. 2012b).

Vaisala's GLD360 network determines lightning locations using both time of arrival and magnetic-direction finding at three or more sensors (Said et al. 2010; Said and Murphy 2016). The lightning 'effective' peak currents are estimated from the measured strength of the VLF electric field and a propagation model accounting for attenuation in the Earth-ionosphere waveguide (Said 2018). These estimates are typically within 25–50% of peak currents measured from rocket-triggered lightning (Mallick et al. 2014) and the National Lightning Detection Network (Said 2018). GLD360 does not explicitly distinguish in-cloud and cloud-to-ground lightning, but we use the threshold defined by Biagi et al. (2007) to infer that lower peak currents (weaker than ± 15 kA) are statistically more likely to originate from in-cloud lightning (Fig. 3b). The GLD360 has a detection efficiency in the range of 67–80% for cloud-to-ground lightning over the continental United States (Said et al. 2013; Mallick et al. 2014; Said and Murphy 2016). Poorer network performance should be expected around Bogoslof due to fewer sensors in the region, but we estimate the cloud-to-ground lightning detection efficiency was still above ~ 70%, using the modeling approach of Pessi et al. (2009).

In addition to the GLD360 production dataset described above, which captured lightning with peak currents as small as 2 kA during the Bogoslof eruption, we were also curious about the weakest electrical activity that could be detected for early warning. We applied the *sparse network technique* developed by Lapierre et al. (2018), using only the two closest GLD360 sensors to Bogoslof, and assuming the signals originated within 100 km of the vent. The advantage of the two-sensor solution is improved sensitivity to low-current lightning (< 2 kA)—in this case, it allowed earlier detection of several explosions and more than doubled the total strokes detected (Table 1). Disadvantages include poorer location accuracy and a noisier dataset, increasing false positives by ~ 1

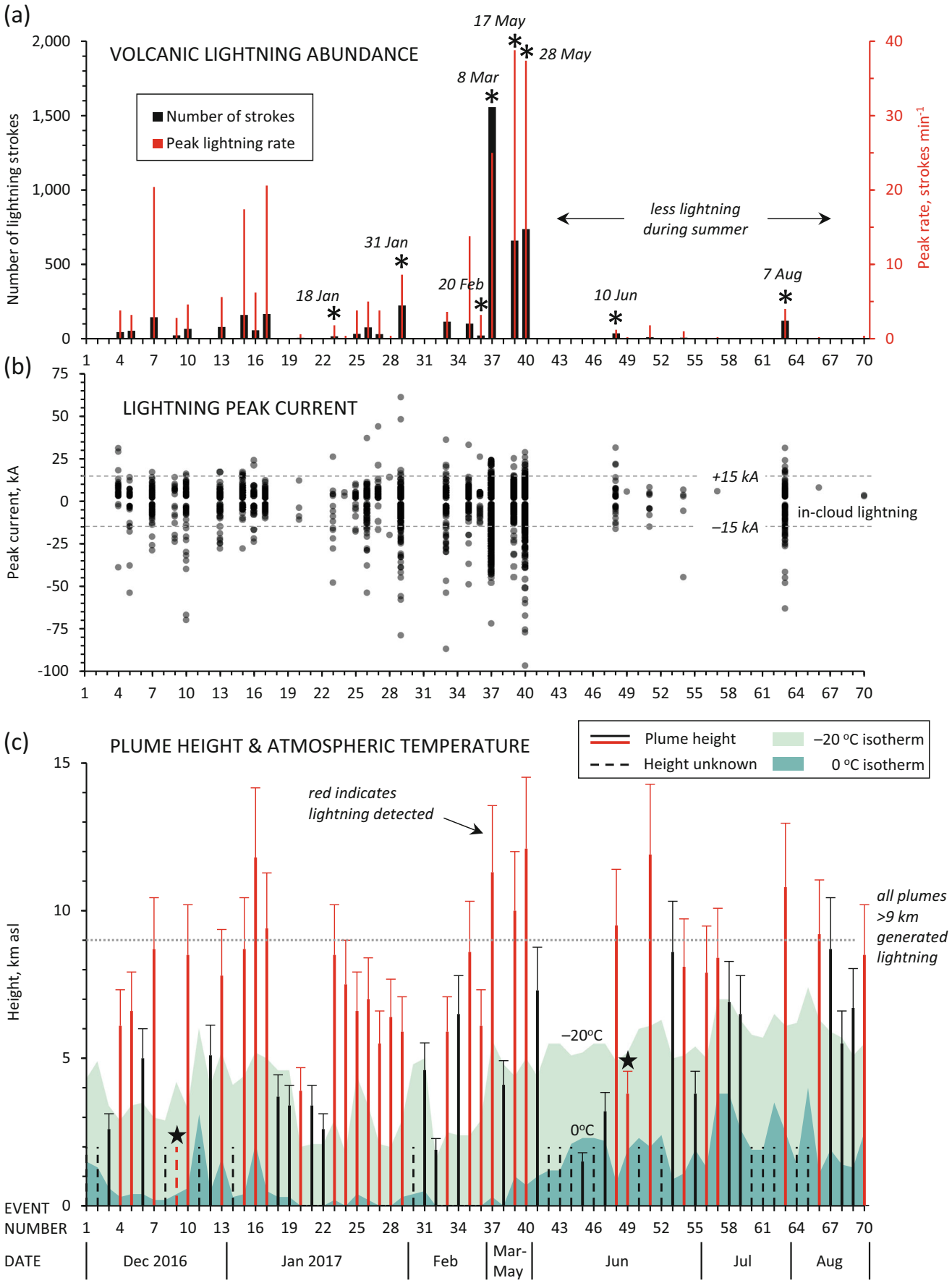
(a)
VOLCANIC LIGHTNING ABUNDANCE
Number of strokes
Peak lightning rate
Number of lightning strokes
Peak rate, strokes min-1
17 May
28 May
8 Mar
31 Jan
18 Jan
20 Feb
10 Jun
7 Aug
less lightning during summer
(b)
LIGHTNING PEAK CURRENT
Peak current, kA
+15 kA
–15 kA
in-cloud lightning
(c)
PLUME HEIGHT & ATMOSPHERIC TEMPERATURE
Plume height
Height unknown
–20 °C isotherm
0 °C isotherm
red indicates lightning detected
all plumes >9 km generated lightning
–20°C
0°C
Height, km asl
EVENT NUMBER
DATE
Dec 2016
Jan 2017
Feb
Mar-May
Jun
Jul
Aug

◀ **Fig. 3** Overview of volcanic lightning, plume heights, and atmospheric temperatures during the 2016–2017 eruption of Bogoslof. **a** Lightning abundance shown as number of strokes and peak rate (strokes min^{-1}) during each of the 70 explosive events from the combined WWLLN and GLD360 datasets. Asterisks highlight the case studies examined in detail. **b** Distribution of peak currents and lightning polarity during each explosive event; low-current lightning is inferred to be in-cloud. **c** Satellite-detected maximum plume height from each event, shown as vertical bars; plumes that generated lightning are shown in red; error bars give 20% uncertainty. Unknown heights (dashed bars) are given an arbitrary value of 2 km. Shading indicates where atmospheric temperatures over Bogoslof volcano reached 0 °C and − 20 °C, as determined from ERA-Interim reanalysis. Note that lightning from event 56 (2 July) was detected only by glitches on infrasound cables, described in Haney et al. (2020). Stars indicate the two plumes that generated lightning without clear evidence of rising above the − 20 °C isotherm (events 9 and 49). However, both may have been higher than suggested by this plot—event 9 is pictured in Fig. 2d, and event 49 injected an SO_2 cloud to 6.4 km asl (Lopez et al. 2020). Lightning was generated by all plumes measured above 9 km asl (not including the height uncertainties)

stroke min^{-1}. To mitigate these effects, we ignored the extra detections unless they were (1) associated with rates > 5 per min or (2) confirmed by a third sensor. Results of the two-sensor solution are described separately in this paper (Table 1), and unless otherwise specified, GLD360 data come from the production dataset.

Lightning data from the WWLLN and GLD360 networks were cross-correlated to identify duplicate measurements of the same stroke. Using this method, WWLLN detections were removed if they overlapped within 5 km and 1 ms of a GLD360 detection. Lightning from non-volcanic thunderstorms was also removed, and this process was relatively straightforward for two reasons: (1) most of the explosive events were isolated, short-lived events, typically tens of minutes or less; and (2) ordinary lightning is uncommon in Alaska—in our case, there were < 30 non-volcanic lightning strokes within 100 km of Bogolsof during the 9-month eruption. Thus, volcanic and non-volcanic lightning rarely coincided in time and space. Average lightning stroke rates were calculated in non-overlapping, 5-min windows over the entire eruption, and results were divided by 5 min to obtain the average strokes per min (Fig. 3; Table 1). For this investigation, we classified the eruption plumes as *electrically active* if volcanic lightning was detected by at least one of the global lightning networks or by the cable glitches reported in Haney et al. (2020). We recognize that even the plumes that failed to produce detectable lightning may still have carried a charge, and some probably generated weak discharges that were below our detection threshold (peak currents ~ 2 kA or less).

Volcanic plume heights were detected by satellite from Schneider et al. (2020) and Lopez et al. (2020). Ash plume heights were determined primarily by cloud-top temperatures in thermal infrared, or displacement measurements in visible satellite images (Schneider et al. 2020). For cases in which plume heights were not measurable due to regional cloud cover or untimely satellite passes, we used the mean height of SO_2 clouds from Lopez et al. (2020). In reality, the SO_2 gas often separates from the ash component, particularly during phreatomagmatic eruptions (Schneider et al. 1999)—a notable example is the 2011 eruption of Grímsvötn, Iceland (Moxnes et al. 2014). So we emphasize that the SO_2 heights only give a rough approximation of ash injection height. However, Lopez et al. (2020) showed that for the majority of cases (> 80%), the two methods were within 2 km of each other. Error bars of 20% are shown for all plume heights in Fig. 3c, based on a comparison of independent satellite methods by Schneider et al. (2020). The 20% uncertainty accounts for an error of ~ 2 km for plumes that reach 10 km asl, and generally more tightly constrained heights for lower-level plumes (see Schneider et al. (2020) for additional details).

To reconstruct the development of Bogoslof's water-rich plumes, we used the 1D model Plumeria, which accounts for water phase changes (Mastin 2007) and effects of the background wind field (Mastin 2014). Plumeria calculates mean properties of a steady-state volcanic plume as a function of height, and we implemented a freezing parameterization based on the experimental work of Schill et al. (2015) to handle heterogeneous ice nucleation in the presence of volcanic ash and sea aerosols. Using these assumptions, liquid water and ice coexist in the plume over temperatures of − 15 °C and − 23 °C. Model inputs include the atmospheric profile over Bogoslof from ECMWF ERA-Interim reanalysis, as in Schwaiger et al. (2020), and eruption source parameters such as plume height and water content, based on explosive event 40 from 28 May 2017. We varied the amount of external water incorporated into the plume from 0 to 30 wt.% to investigate how different amounts of magma-water interaction would affect the plume dimensions, freezing level, and airborne concentrations of hydrometeors. Results from the full suite of model runs are available in Supplementary Material (Fig. S1 and Table S1).

Overview of lightning characteristics

The combined database from WWLLN and GLD360 contains > 4550 volcanic lightning strokes over the 2016–2017 eruptive sequence (Supplementary Material). Figure 1 shows that the lightning occurred within a fairly restricted area around the volcano—98% of the strokes were within 25 km of Bogoslof (Fig. 1b). The modest spatial footprint of electrical activity is consistent with the generally low plume heights (maximum ~ 12 km asl) compared to more powerful, examples from Kelud and Calbuco, which both exceeded 20 km asl (Van Eaton et al. 2016; Hargie et al. 2019). Figure 3 provides an overview of volcanic, atmospheric, and lightning properties for the full eruptive sequence. Table 1 summarizes

Table 1 Eruption parameters and volcanic lightning characteristics of 70 explosive events from the 2016–2017 eruption of Bogoslof, Alaska. All times in UTC. Bold font denotes case-studies described in detail in the text; "–" indicates no detection. Onset of eruptive behavior is from Coombs et al. (2019). Lightning parameters are shown from the two-sensor solutions (GLD360 only) and from the combined WWLLN and GLD360 dataset. "*" indicates when the two-sensor solutions detected activity earlier than the combined dataset. Peak stroke rates are averaged over 5-min intervals. Percentages of in-cloud lightning are defined by peak currents weaker than ± 15 kA from GLD360 data. Infrasound detection durations give the sum of time windows containing above-background infrasound on the Okmok microphone array; note that these are minimum durations in most cases due to uncertainties in infrasound path effects and wind noise, as discussed in Lyons et al. (2020). Plume heights are from Schneider et al. (2020) and Lopez et al. (2020), with the exception of events 37 and 40, which use maximum heights from Himawari-8, based on retrievals from NOAA/NESDIS (Michael Pavolonis, personal communication). Mass eruption rates in kg/s (MER) are determined from the empirical plume height scaling relationship $M = 140 \times H^{4.15}$ where H is the plume height in km (Eq. 2 of Mastin 2014). Eruption rates are maximum values because they use the maximum plume height observation for each event. Lightning detected as electrical glitches (e.g., during event 56) are described in Haney et al. (2020)

Event #	Event date	Onset time of eruptive behavior	Lightning from GLD two-sensor solutions		Lightning from combined WWLLN + GLD360 dataset					Infrasound detection duration, min	Max plume height, km asl	Satellite used for plume height	Max eruption rate, kg/s
			Onset time (* indicates early detection)	# of strokes	Onset time	Lightning duration, min	# of strokes	Peak rate, strokes per min	% in-cloud lightning (GLD360 only)				
1	12 Dec 2016	12:40	–	–	–	–	–	–	–	7.0	–	GOES	–
2	12 Dec 2016	17:44	–	–	–	–	–	–	–	125.0	–	GOES	–
3	14 Dec 2016	22:10	–	–	–	–	–	–	–	–	2.6	Sentinel	7×10^3
4	16 Dec 2016	18:39	18:36	163	18:36	15	45	3.8	90	1.5	6.1	GOES	3×10^5
5	19 Dec 2016	15:14	15:49	190	15:49	45	53	3.2	91	–	6.6	IASI (SO_2)	3×10^5
6	21 Dec 2016	0:38	–	–	–	–	–	–	–	–	5.0	GOES	1×10^5
7	22 Dec 2016	1:22	1:27	285	1:28	28	144	20.4	96	9.5	8.7	AVHRR	1×10^6
8	22 Dec 2016	11:41	–	–	–	–	–	–	–	–	–	GOES	–
9	23 Dec 2016	18:33	*18:39	58	18:43	5	22	2.8	83	–	–	GOES	–
10	26 Dec 2016	23:22	*23:28	159	23:33	42	66	4.6	81	–	8.5	AVHRR	1×10^6
11	29 Dec 2016	3:29	–	–	–	–	–	–	–	–	–	GOES	–
12	30 Dec 2016	8:35	–	–	–	–	–	–	–	–	5.1	GOES	1×10^5
13	31 Dec 2016	7:33	*7:29	121	7:30	32	79	5.6	85	–	7.8	IASI (SO_2)	7×10^5
14	2 Jan 2017	22:56	–	–	–	–	–	–	–	–	–	GOES	–
15	4 Jan 2017	6:19	6:19	494	6:20	18	160	17.4	98	0.5	8.7	GOES	1×10^6
16	5 Jan 2017	22:30	22:29	133	22:25	16	57	6.2	85	4.5	11.8	VIIRS	4×10^6
17	9 Jan 2017	7:26	*7:59	419	8:00	16	166	20.6	100	39.5	9.4	VIIRS	2×10^6
18	12 Jan 2017	20:23	–	–	–	–	–	–	–	–	3.7	GOES	3×10^4
19	12 Jan 2017	21:31	–	–	–	–	–	–	–	–	3.4	GOES	2×10^4
20	15 Jan 2017	6:40	*7:12	34	7:16	25	6	0.6	100	3.0	3.9	IASI (SO_2)	4×10^4
21	17 Jan 2017	14:30	–	–	–	–	–	–	–	–	3.4	GOES	2×10^4
22	17 Jan 2017	16:40	–	–	–	–	–	–	–	–	2.6	GOES	7×10^3
23	**18 Jan 2017**	**22:19**	***22:24**	**81**	**22:26**	**13**	**16**	**1.8**	**57**	**–**	**8.5**	**MODIS**	$\mathbf{1 \times 10^6}$
24	20 Jan 2017	22:18	22:24	12	22:18	8	3	0.4	100	1.0	7.5	MODIS	6×10^5
25	22 Jan 2017	23:00	23:02	128	23:02	13	33	3.8	93	–	6.6	GOES	4×10^5
26	24 Jan 2017	13:51	*13:53	184	13:57	44	76	5.0	85	2.5	7.0	AVHRR	5×10^5
27	26 Jan 2017	15:49	15:49	98	15:50	24	31	3.8	88	–	5.5	GOES	2×10^5
28	27 Jan 2017	17:25	*17:35	23	17:38	4	3	0.4	50	8.5	6.4	AVHRR	3×10^5
29	**31 Jan 2017**	**5:18**	***6:38**	**649**	**6:38**	**327**	**223**	**8.6**	**84**	**117.5**	**5.9**	**MODIS**	$\mathbf{2 \times 10^5}$

Table 1 (continued)

Event #	Event date	Onset time of eruptive behavior	Lightning from GLD two-sensor solutions		Lightning from combined WWLLN + GLD360 dataset					Infrasound detection duration, min	Max plume height, km asl	Satellite used for plume height	Max eruption rate, kg/s
			Onset time (* indicates early detection)	# of strokes	Onset time	Lightning duration, min	# of strokes	Peak rate, strokes per min	% in-cloud lightning (GLD360 only)				
30	3 Feb 2017	14:00	–	–	–	–	–	–	–	–	–	AVHRR	–
31	4 Feb 2017	1:50	–	–	–	–	–	–	–	–	*4.6*	GOES	8×10^4
32	13 Feb 2017	16:24	–	–	–	–	–	–	–	–	1.9	IASI (SO_2)	2×10^3
33	17 Feb 2017	19:05	*19:16	225	19:22	67	114	3.6	76	7.0	5.9	AVHRR	2×10^5
34	18 Feb 2017	0:34	–	–	–	–	–	–	–	–	6.5	AVHRR	3×10^5
35	18 Feb 2017	14:00	*14:02	235	14:03	10	101	13.8	93	–	8.6	AVHRR	1×10^6
36	**20 Feb 2017**	**2:08**	**2:12**	**68**	**2:13**	**14**	**21**	**3.2**	**95**	**18.0**	**6.1**	**GOES**	$\mathbf{3 \times 10^5}$
37	**8 Mar 2017**	**7:37**	***7:59**	**2690**	**8:00**	**158**	**1557**	**25.0**	**91**	**163.5**	**11.3**	**Himawari-8**	$\mathbf{3 \times 10^6}$
38	13 Mar 2017	11:31	–	–	–	–	–	–	–	1.5	4.1	GOES	5×10^4
39	**17 May 2017**	**6:29**	***6:43**	**1637**	**6:52**	**67**	**660**	**38.8**	**98**	**66.5**	**10.0**	**GOES**	$\mathbf{2 \times 10^6}$
40	**28 May 2017**	**22:16**	***22:36**	**1845**	**22:37**	**35**	**737**	**37.4**	**90**	**24.5**	**12.1**	**Himawari-8**	$\mathbf{4 \times 10^6}$
41	1 Jun 2017	2:44	–	–	–	–	–	–	–		7.3	GOES	5×10^5
42	5 Jun 2017	15:50	–	–		–	–	–	–	0.5	–	GOES	–
43	5 Jun 2017	20:29	–	–		–	–	–	–	–	–	GOES	–
44	6 Jun 2017	13:59	–	–		–	–	–	–	1.0	–	GOES	–
45	7 Jun 2017	14:28	–	–		–	–	–	–	3.5	1.5	AVHRR	8×10^2
46	8 Jun 2017	5:28	–	–		–	–	–	–	–	–	GOES	–
47	9 Jun 2017	0:58	–	–		–	–	–	–	0.5	3.2	GOES	2×10^4
48	**10 Jun 2017**	**9:58**	**12:16**	**94**	**12:16**	**56**	**36**	**1.2**	**87**	**83.5**	**9.5**	**VIIRS**	$\mathbf{2 \times 10^6}$
49	13 Jun 2017	1:44	1:56	7	1:56	1	1	0.2	100	42.0	3.8 / 6.4	AVHRR / SO2	4×10^4
50	13 Jun 2017	16:15	–	–		–	–	–	–	1.5	–	GOES	–
51	24 Jun 2017	0:49	*0:57	164	1:04	4	10	1.8	89	5.0	11.9	AVHRR	4×10^6
52	24 Jun 2017	3:19	–	–		–	–	–	–	10.5	–	GOES	–
53	27 Jun 2017	0:44	–	–		–	–	–	–	–	8.6	AVHRR	1×10^6
54	27 Jun 2017	11:17	*11:28	40	11:32	6	7	1.0	80	–	8.1	GOES, MODIS	8×10^5
55	30 Jun 2017	1:34	–	–		–	–	–	–	2.0	3.8	GOES	4×10^4
56	2 Jul 2017	20:47	–	–	Event 56 lightning detected by glitches on Okmok array at 20:48					1.5	7.9	AVHRR	7×10^5
57	5 Jul 2017	0:51	0:53	3	0:54	1	1	0.2	100	10.0	8.4	AVHRR	1×10^6
58	5 Jul 2017	3:05	–	–		–	–	–	–	5.5	6.9	GOES	4×10^5
59	8 Jul 2017	18:15	–	–		–	–	–	–	–	6.5	GOES	3×10^5
60	10 Jul 2017	7:46	–	–		–	–	–	–	10.0	–	GOES	–
61	10 Jul 2017	17:59	–	–		–	–	–	–	6.5	–	GOES	–
62	11 Jul 2017	1:07	–	–		–	–	–	–	–		GOES	–
63	**7 Aug 2017**	**18:21**	***18:49**	**529**	**18:56**	**128**	**121**	**4.0**	**79**	**10.0**	**10.8**	**AVHRR**	$\mathbf{3 \times 10^6}$
64	14 Aug 2017	16:49	–	–		–	–	–	–	–		GOES	–

Table 1 (continued)

Event #	Event date	Onset time of eruptive behavior	Lightning from GLD two-sensor solutions		Lightning from combined WWLLN + GLD360 dataset					Infrasound detection duration, min	Max plume height, km asl	Satellite used for plume height	Max eruption rate, kg/s
			Onset time (* indicates early detection)	# of strokes	Onset time	Lightning duration, min	# of strokes	Peak rate, strokes per min	% in-cloud lightning (GLD360 only)				
65	22 Aug 2017	12:06	–	–		–	–	–	–	1.5	–	GOES	–
66	27 Aug 2017	0:28	*0:30	20	0:32	1	1	0.2	100	4.0	9.2	AVHRR	1×10^6
67	27 Aug 2017	23:08	–	–		–	–	–	–	1.5	8.7	MODIS	1×10^6
68	28 Aug 2017	11:22	–	–		–	–	–	–	1.5	5.5	IASI (SO_2)	2×10^5
69	28 Aug 2017	19:17	–	–		–	–	–	–	–	6.7	GOES	4×10^5
70	30 Aug 2017	12:30	*12:58	13		13:00	7	2	0.4	100	8.5	GOEs	1×10^6

key parameters, including mass eruption rates based on empirical relationships to plume height (Mastin et al. 2009; Mastin 2014).

An immediate observation is that fewer than half of the explosive events generated lightning (32 out of 70 events). Figure 3c shows that all plumes rising > 9 km asl also produced lightning, along with 90% of the plumes > 8 km (18 out of 20). Based on this finding, the highest plumes were clearly more likely to become lightning-rich.

However, there is only a weak linear correlation across the full range of plume heights observed (Fig. 4a). Roughly 24% of the variability in lightning rate can be explained by the maximum plume height (red dashed line, Fig. 4a). Some of the scatter is from a suite of explosions that produced less lightning than expected from plume height alone (7–12 km). One explanation is that these events were short-lived—Fig. 4b shows that the briefest explosions (< 5 min, based on infrasound detection duration) were less likely to generate lightning. But there is also a seasonal effect visible in Fig. 3a. Notice how volcanic lightning decreased during the late spring and summertime events, despite similar maximum plume heights (Fig. 3a). We initially considered the possibility that the lightning sensors were saturated by enhanced global lightning during the northern hemisphere summer, but found a negligible impact (no relevant sensors were down for more than a few minutes). This suggests a 'real' decrease in lightning generation from the summertime eruption plumes. Two notable changes were taking place during these later events. First, the explosions became shorter-lived—average infrasound detection durations decreased by 50% after event 38 on 13 March 2017 (Table 1; Lyons et al. 2020). Many of these short-lived explosions failed to produce detectable lightning despite (briefly) reaching a high altitude (Fig. 4b). Second, the atmosphere became seasonably warmer during the spring and summer (shaded regions in Fig. 3c). Warmer atmospheric temperatures require plumes to rise higher to reach freezing levels where ice charging can occur, as observed during the 2010 eruption of Eyjafjallajökull in Iceland (Arason et al. 2011). Arason et al. (2011) identified − 20 °C as a possible threshold for volcanic plumes, beyond which the plume cools sufficiently to create a mixed-phase region of graupel, ice crystals, and supercooled liquid drops—the crucial ingredients for thunderstorm-style charging.

Figure 3c compares the height of electrically-active plumes with the height of the − 20 °C and 0 °C isotherms above Bogoslof, determined from ERA-Interim reanalysis (Schwaiger et al. 2020). Among the lightning producers, shown as red bars in Fig. 3c, all but two injected into the freezing level of the atmosphere (stars in Fig. 3c). One of the exceptions is event 9 on 23 Dec 2016, which generated

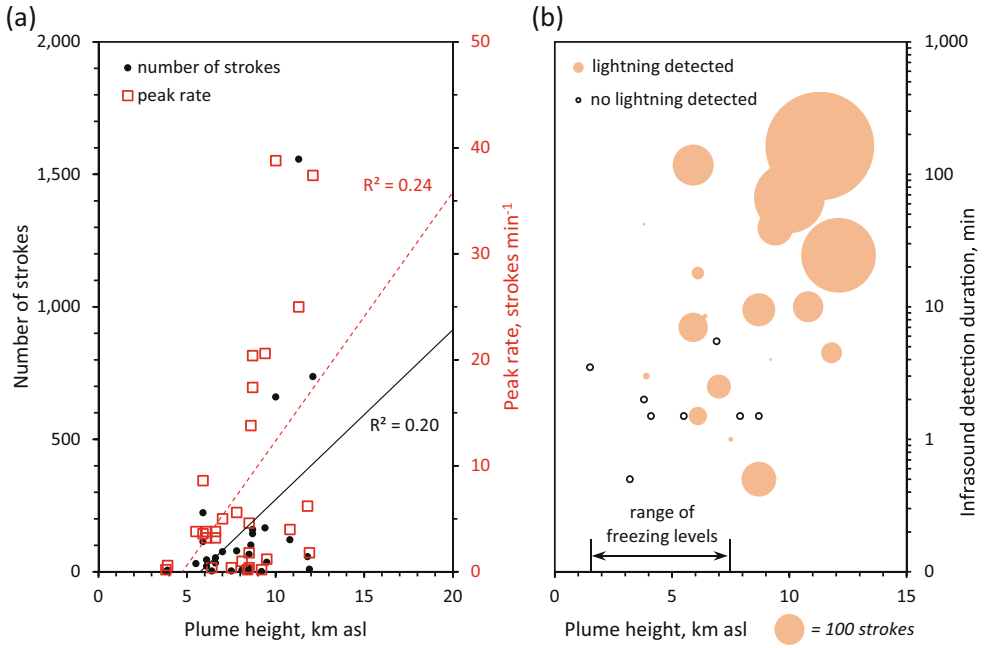

Fig. 4 Relationships between eruption dynamics and volcanic lightning during individual eruptive events, using the combined WWLLN and GLD360 dataset. **a** Maximum plume height shows a weak linear relationship to the number of strokes (black dots; $R^2 = 0.20$; p value 0.01) and peak lightning rate (red squares; $R^2 = 0.24$; p value 0.01). All events with detectable lightning and plume heights are shown ($n = 30$). Statistical details provided in Supplementary Table S2. **b** Plumes with and without detected lightning, plotted by height and duration of ash emissions (approximated from infrasound detection durations; Table 1). Orange circles are area-scaled to the number of lightning strokes. All explosive events with measured plume heights and infrasound detection durations are included in the plot ($n = 29$). Range of freezing levels gives height of − 20 °C temperatures above Bogoslof volcano across the entire eruption. Note that explosive events lasting > 5 min and with plume heights > 9 km are more likely to produce abundant lightning. An important caveat is that the plume heights in this figure represent only a single snapshot in time, ignoring the height variations during individual explosions

22 lightning strokes, and was not observed in satellite due to regional cloud cover at least 9 km altitude. But based on the distant photographs of a towering, incandescent column penetrating the cloud deck (Fig. 2d), it probably did rise higher than the local freezing level of ~ 4 km. The other exception is event 49 on 13 June 2017, which produced only one in-cloud lightning stroke (and two electrical glitches) without rising above the freezing level of 5.2 km. However, its SO_2 cloud was detected at heights of 6.4 km ~ 4 h after the end of the explosive event (Lopez et al. 2020), so some amount of higher-level injection is possible. Figure 3c also reveals that nine plumes rose above the − 20 °C level without producing any detectable lightning (events 6, 12, 21, 22, 34, 41, 53, 67, and 69). These were short-lived events (infrasound detection durations < 2 min or not detected at all; Table 1), which produced small, rapidly dissipating clouds (Schneider et al. 2020). We suspect that these intense, but brief, explosions were not sustained long enough to create globally-detectable lightning. Following from these general observations, the question remains if ice formation played a governing role in the electrification of Bogoslof's plumes. To examine the issue, we consider eight case studies in finer temporal and spatial resolution.

Detailed case studies

Using eight case studies of electrically-active plumes, we examine the time series of eruption dynamics inferred from plume heights, plume morphology, and infrasound frequency. Comparing these observations with lightning stroke rates, peak currents, and results from 1D plume modeling allows us to consider how electrical activity is influenced by (1) plumes rising above the local freezing level and (2) submarine vs. subaerial vent conditions.

Two moderate-intensity, submarine explosions

First, we examine two of the most electrically active explosions of the 2016–2017 eruption. Event 39 (17 May) and event 40 (28 May) produced some of the highest plumes of the eruption, although they were both moderate intensity in terms of mass eruption rate (~ 10^6 kg s^{-1}, using empirical plume height scaling relationships; Table 1). Shallow seawater likely covered the vent for the entire duration of these explosions, based on the persistent, low frequency infrasound (Fee et al. 2020). Figure 5 illustrates the plume dynamics and lightning from event 40 on 28 May. Notice the burst of low-

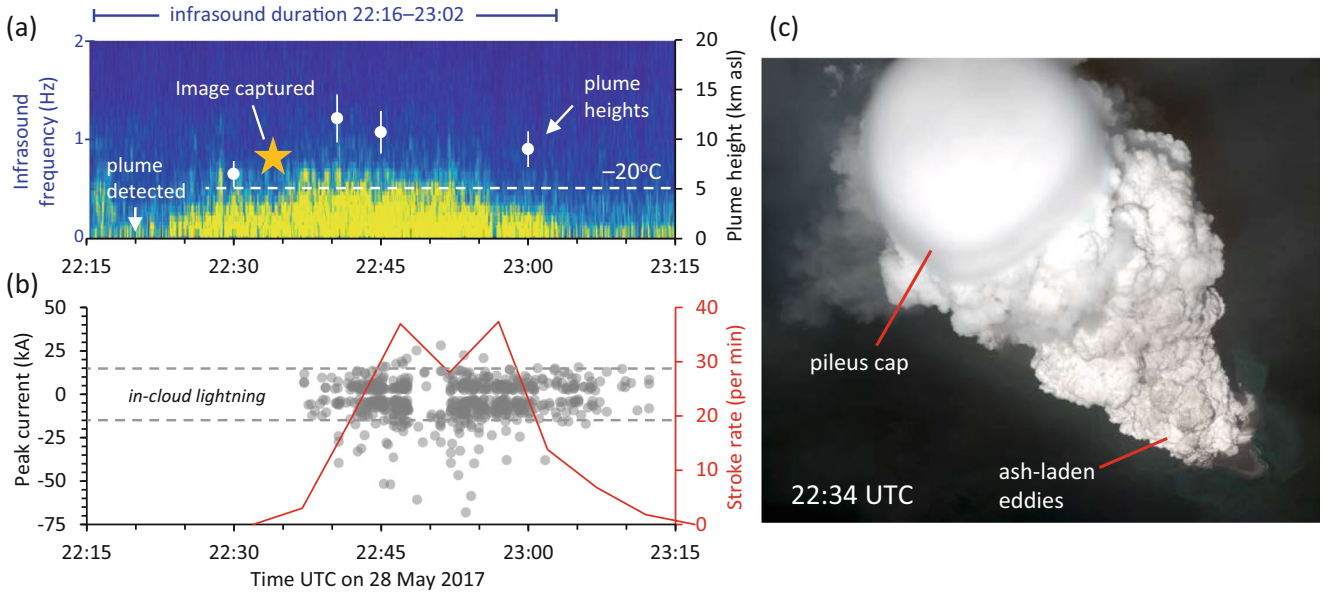

Fig. 5 Plume dynamics and lightning generation from the shallow submarine explosion on 28 May 2017 (event 40). **a** Time series of plume heights (white circles; note values on right axis) overlain with infrasound frequency (yellow-blue spectrogram; yellow indicates more intense energy). Dashed horizontal line shows height of the −20 °C freezing level of the atmosphere. Labeled *infrasound duration* gives the start and end time of above-background acoustic signals detected on the Okmok array. **b** Time series of volcanic lightning, showing peak currents (gray circles) from GLD360 data and lightning stroke rates (red line) in 5-min intervals from the combined WWLLN + GLD360 dataset. Peak currents weaker than ± 15 kA inferred to be in-cloud lightning (dashed gray lines). The gap in lightning data from 22:48 to 22:52 is due to a temporary drop in signal from a GLD360 sensor. **c** Worldview satellite image at 22:34 UTC, captured just after the plume rose above the freezing level, and 2 min before producing detectable lightning. Note the white color, particularly toward the top of the column, and presence of a pileus cap cloud, indicating formation of condensed water and ice crystals. Refer to full size digital image for details: https://avo.alaska.edu/images/image.php?id=109261. Image provided under a Digital Globe NextView License

frequency infrasound (yellow color) at 22:16 UTC, signaling the start of explosive eruption through seawater (Fig. 5a). The beginning of an eruption column was first observed at 22:20 in visible satellite imagery (Himawari-8), but was too small to obtain height information. Figure 5a shows that acoustic energy increased over the next 10 min, as the vertical ash column rose to a height of 6.5 km asl by 22:30, which is within uncertainty of the local freezing level (dashed white line in Fig. 5a). Note that the plume was still electrically quiet at this point, despite its substantial height (Fig. 5b). Moments later, a fortuitous pass of the Worldview satellite imaged the rising column, which was only 2 min away from becoming an intense lightning storm (Fig. 5c). The plume morphology reveals a well-mixed, turbulent column that had not yet reached the level of neutral buoyancy or formed an umbrella cloud. The color of the plume grades from light, ashy gray at its base (label in Fig. 5c) to stark white toward the top, reflecting both the high proportion of seawater incorporated into the plume, and the rapid condensation of water in the near-vent area. Similar processes were observed during the Icelandic eruption of Surtsey, when the plume "abruptly turned white as the steam cooled and condensed" (Anderson et al. 1965).

At Surtsey, Thorarinsson (1967) described icy precipitation falling from the water-rich plumes, noting "tephra fell in hail showers, one grain of tephra within each hailstone". This relates to the Bogoslof plume pictured in Fig. 5c because nucleation of water and ice on the ash particles obscured their recognition in both the visible (Fig. 5c) and infrared wavelengths (Schneider et al. 2020). The cloud did not drift toward land, so there was no recognizable ash fall, but the presence of ash-laden eddies in the lower eruption column (Fig. 5c), and production of a sizeable SO_2 cloud (Lopez et al. 2020), including several aircraft encounters (Coombs et al. 2019), support a phreatomagmatic, ash-rich source rather than an ash-free steam plume. A final observation from Fig. 5c is that the top of the rising column is capped by a *pileus cloud*—a smooth, gauzy veil made of condensed water and, likely, ice crystals (Garrett et al. 2006). In meteorology, pileus clouds develop when parcels of moist air are forced ahead of strong updrafts. A prominent example occurred during the 2009 eruption of Sarychev Peak, Russia, photographed from the International Space Station (Rybin et al. 2011; their Fig. 5). Taken together, these features point to condensed water and ice formation within the volcanic plume in the minutes leading up to lightning generation. After 22:34 UTC, the column continued to rise into the stratosphere, with an overshooting top reaching 12 km by 22:40.

The finding that condensation occurred close to sea level (image in Fig. 5c) provides some useful constraints on water contents in the volcanic plume. A sensitivity analysis using the 1D model Plumeria shows that ~25 wt.% external water

was required for low-altitude condensation on 28 May (Supplementary Fig. S1). The model scenario in Fig. 6 reveals several interesting features. For one, it confirms that freezing would have taken place at heights of ~ 7 km in the plume (Fig. 6a, b), coinciding with the time of the Worldview image and onset of lightning generation (Fig. 5a–c). It also shows a mixed-phase region from 7 to 8 km (shading in Fig. 6b), where liquid water and ice coexist within vigorous updrafts of 40–50 m/s (Fig. 6c). These conditions are ripe for collisional ice charging (Deierling et al. 2008). In fact, the extremely high liquid water contents (6–9 g m^{-3}) are on par with those in the most severe thunderstorms, > 5 g m^{-3} (Williams 1995; Loney et al. 2002). Under this scenario, it is likely that ice-charging would take an active role in plume electrification.

Bogoslof's event 39 on 17 May began generating low-frequency infrasound at 6:29 UTC (Fig. 7a). But due to an extensive weather system over the region, the white, ice-rich plume merged with background clouds, making it difficult to track precise changes in plume height during the > 1 h of lightning activity. There were several weak lightning strokes detected around 6:43 UTC using the high-sensitivity, two-sensor GLD360 method (lightning symbol in Fig. 7b). Around this time, a satellite pass at 6:45 UTC showed the plume still apparently below the cloud deck, which was ~ 5 km (note freezing level at 4.4 km; dashed line in Fig. 7a). After 6:57 UTC, all of the available satellite retrievals show injection to 8–10 km asl, which is well above the freezing level. Despite the cloud's white color and absence of a brightness temperature difference in multispectral satellite data, it was indeed ash-rich, depositing ash fall in the village of Nikolski ~ 124 km southwest. The fall deposits contained juvenile, vesicular glass (Loewen et al. 2019). Peak lightning rates of ~ 39 min^{-1} coincide with the strongest infrasound energies during this event from 7:30–7:50, and almost all of the lightning was in-cloud (98%).

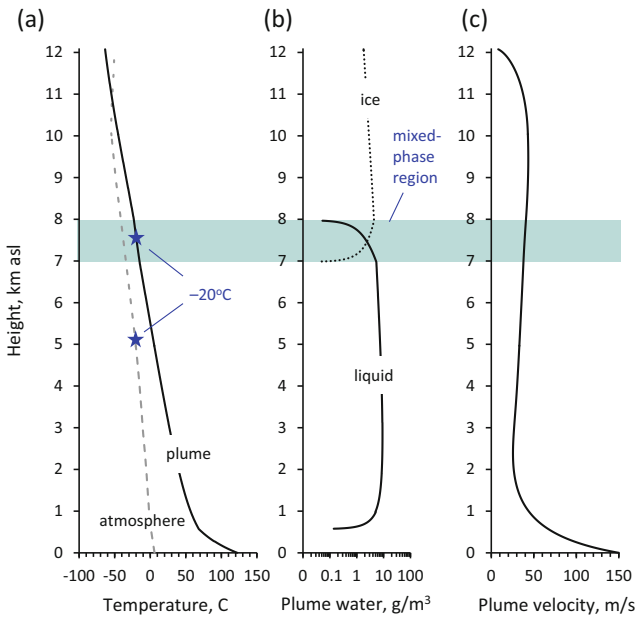

Fig. 6 Results of 1D volcanic plume modeling for Bogoslof's explosive event 40 on 28 May 2017. Model inputs use a maximum plume height of 12.1 km, initial magma temperature 1000 °C, and seawater content of 25 wt.%. **a** Temperature profiles of the background atmosphere (dashed line) and volcanic plume (solid line) show the heights of − 20 °C temperatures (blue stars), and persistently warmer temperatures in the plume until undercooling occurs above 11 km. **b** Modeled water contents reveal a mixed-phase region at heights of 7–8 km (shaded zone) where high concentrations of liquid water and ice coexist in the plume. **c** Velocity profile indicates updrafts of 40–50 m s^{-1} within the mixed-phase region, promoting the conditions for thunderstorm-style collisional ice charging

These moderate-intensity, shallow submarine explosions provide two consistent observations: (1) both produced high rates of in-cloud lightning > 30–40 strokes min^{-1} once the plumes were well above the − 20 °C isotherm, but not beforehand, and (2) there were considerable delays from the start of eruptive activity (see infrasound onset in Figs. 5a and 7a) to the onset of globally-detectable lightning (~ 20 min each), apparently reflecting the time needed to create the conditions for lightning (discussed further in the section on *volcanic lightning for monitoring*).

Transitions between submarine and emergent activity

Here, we examine four explosive events that transitioned between submarine and subaerial vent conditions (Fig. 8). During three of these (events 29, 37, and 63), the vent "dried out," presumably as the buildup of tephra blocked seawater access (Fee et al. 2020; Waythomas et al. 2020), whereas event 48 on 10 June destroyed a subaerial dome, flooding the vent with seawater partway through eruption. These transitioning explosions provide a means to investigate if explosions through water affected the lightning generation. Figure 8 summarizes lightning data alongside satellite-derived plume heights (white circles) and infrasound frequency (yellow-blue spectrograms). Across these diverse events, three features are evident: (1) they all created long-lasting plumes (> 1 h) straddling the freezing level of the atmosphere, (2) most lightning only became detectable once plume heights exceeded the − 20 °C isotherm (keeping in mind the error bars on the plume heights), and (3) the presence of seawater in the vent had no systematic influence on the timing or intensity of volcanic lightning.

Consider event 29 on 31 Jan 2017 (Fig. 8a). This explosion produced low-level plumes < 6 km asl over a period of 6 h, resulting in ash fall on Unalaska Island. Ash clouds first became visible in satellite at 6:30 UTC while the vent inundated was with seawater, based on the lower-frequency (< 2 Hz) infrasound. During this phase, plume heights were sustained above the − 20 °C isotherm of 3 km asl for ~ 30 mins; yet, there was only weak, in-cloud lightning (1–2 strokes per min). The lightning abruptly shut off after

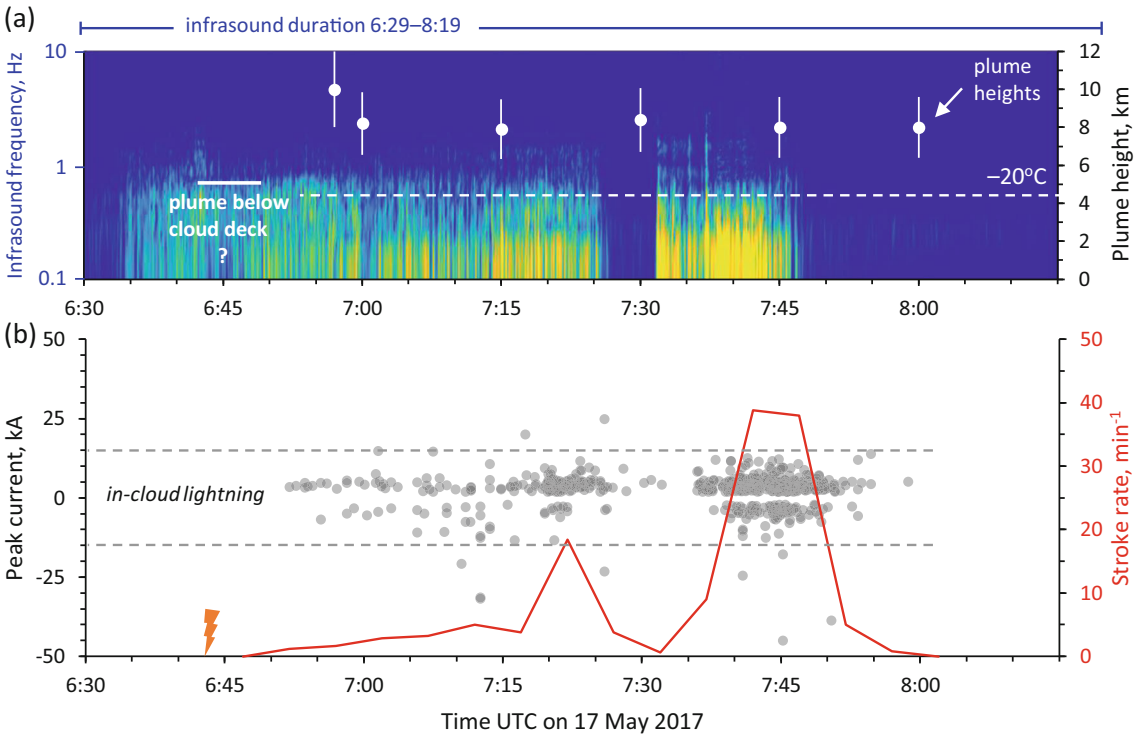

Fig. 7 Plume heights and lightning from the shallow submarine explosion on 17 May 2017 (event 39). **a** Time series of plume heights (white circles) and infrasound frequency (yellow-blue spectrogram; note log scale). **b** Time series of lightning peak currents (gray circles) and strokes per min (red line). Orange lightning symbol shows the onset of two-sensor GLD360 lightning, which detected 5 early strokes from 6:43 to 6:51 UTC. At 6:45, the plume was not yet distinguishable above the regional cloud deck at ~ 5 km. Note − 20 °C isotherm at 4.4 km (dashed white line)

7:00 UTC as the plume dipped below (or near) the − 20 °C isotherm for the remainder of the submarine activity. By 8:40 UTC, higher-frequency infrasound suggests the vent was subaerial. Overall, it appears that the volcanic lightning "turned off and on" depending the plume's height above the freezing level (Fig. 8a). But there were much higher stroke rates during the dry phase of explosive activity, with more cloud-to-ocean lightning (indicated by peak currents greater than ± 15 kA). The plume generated more lightning, despite no significant change in ash cloud heights across the wet-to-dry transition. In this case, it does appear that lightning intensified when there was less water in the vent. A possible explanation is that the abundance of high-conductivity liquid water dissipated the electric charge from particle collisions near the vent. Without sufficient buildup of charge, there cannot be electrical breakdown. However, it is important to observe that this response to water inundation is not consistent across the other explosive events examined (e.g., Figs. 8b–d and 9).

The larger explosion on 8 March (event 37; Fig. 8b) shows little sensitivity to water levels in the vent. With a maximum plume height up to 11.3 km asl, the eruption rate was nearly an order of magnitude higher than event 29 (31 Jan; Table 1). Once the plume rose above the regional cloud deck after 8:10, its height increased over the next few hours, suggesting a gradual increase in mass eruption rate. Lightning was only detected once the plume reached (or exceeded) the − 20 °C isotherm at 5.6 km (Fig. 8b). Lightning stroke rates reached 25 min^{-1}, surpassed only by the eruptive events on 17 May and 28 May. Interestingly, the lightning was dominantly in-cloud judging by low peak currents (> 90% were weaker than ± 15 kA) and showed little change across the wet-to-dry transition. When the vent "dried out" by ~ 9:40 UTC (based on infrasound), plume heights continued to increase by 1–2 km, but without any notable change in lightning rates or peak currents.

Event 48 on 10 June (Fig. 8c), known as the 'dome destroying event,' obliterated a subaerial lava pile about 110 m across (Coombs et al. 2019). Infrasound frequencies suggest that the explosion initiated from a subaerial vent and became progressively more water-rich as the dome disintegrated and allowed seawater to flood the crater. Infrasound started as early as 8:27 UTC, but during this early part of the explosion, no plumes rose above cloud deck at 5–6 km asl (near the freezing level of 4.9 km). Activity occurring below the cloud deck did produce some lightning, indicated by several glitches around 11:15 (Haney et al. 2020). However, the volcanic plume did not rise above surrounding

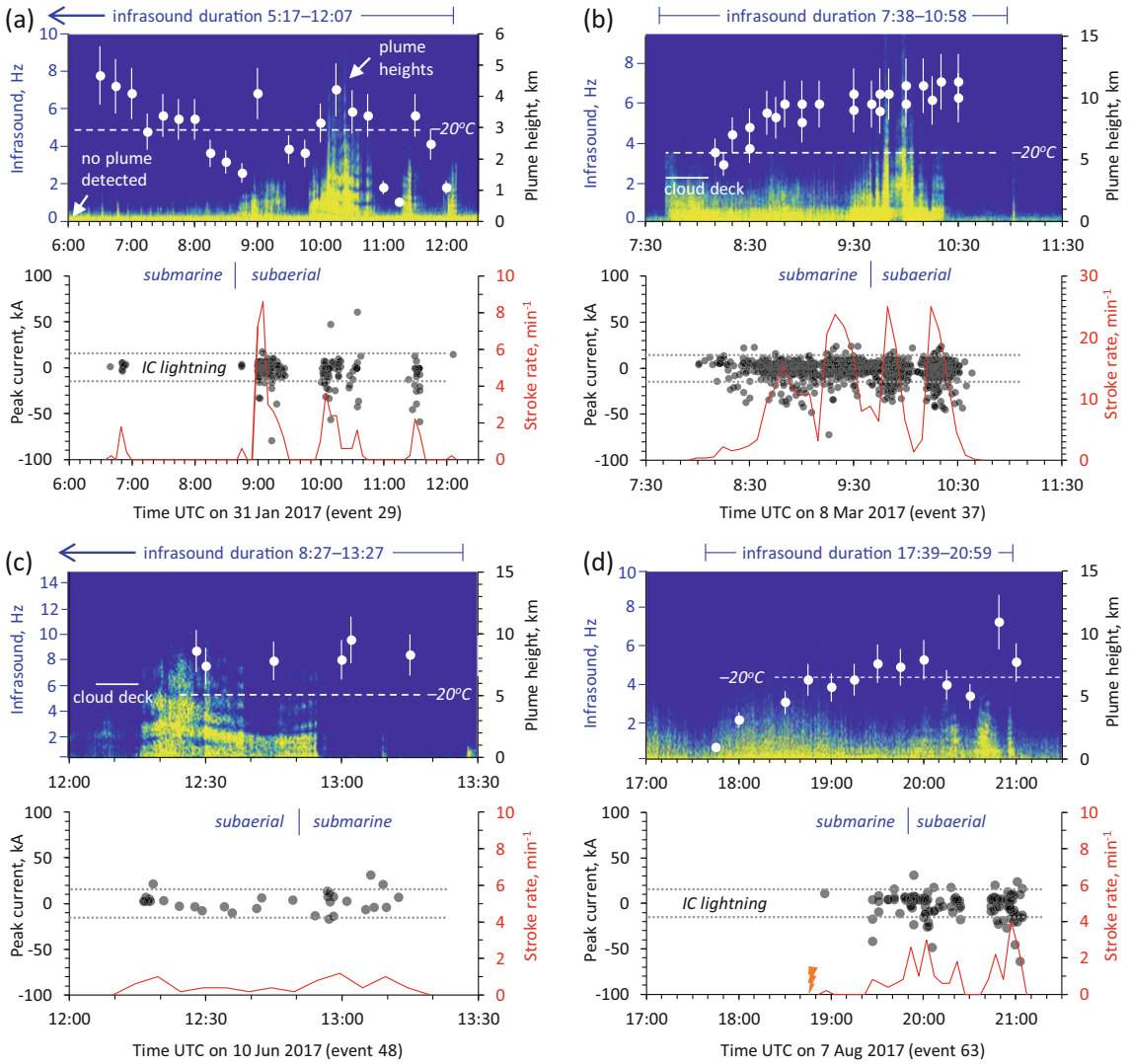

Fig. 8 Plume heights and lightning data from four explosions with shifting seawater access to the vent. Legend as in Fig. 5. Top panels show time-series of plume heights (white circles) and infrasound frequency (yellow-blue spectrograms). The eruptive vent is inferred to be submarine when infrasound frequency drops below 1–2 Hz (Fee et al. 2020). Lower panels show time-series of lightning peak currents (gray circles) and strokes min^{-1} (red line). **a** Event 29 on 31 Jan 2017. **b** Event 37 on 8 March 2017. **c** Event 48 on 10 June 2017; note that electrical glitches were detected around 11:15 UTC, before the ash plume became visible above the cloud deck. **d** Event 63 on 7 August 2017

clouds until after ~ 12:00. Globally detected lightning began at 12:16, and plume heights hovered around 7–8 km asl, producing one of only two *ash signals* (satellite brightness temperature difference) of the entire Bogoslof eruption (Schneider et al. 2020). The ash signal suggests lower ice contents in the plume (which can mask the brightness temperature difference), consistent with an origin from the subaerial dome, rather than from an underwater explosion. When seawater flooded into the vent after ~ 12:50 (based on infrasound), the plume briefly reached its maximum height of 9.5 km asl. But in this case, lightning characteristics appear unchanged by the influx of water (Fig. 8c). Low stroke rates (< 2 min^{-1}), and predominantly in-cloud lightning persist across the dry-to-wet transition.

Event 63 on 7 August 2017 lasted at least 3 h, with a slow-climbing plume that "dried out" toward the end of the activity (Fig. 8d). As the water-rich plume rose above 7 km asl, it produced lightning within minutes of reaching the freezing level (Fig. 8d). Infrasound signals indicate that the vent dried out by 19:50 UTC, likely due to build-up of proximal tephra that blocked seawater access (Coombs et al. 2019). Across the transition period, plume heights remained relatively stable without any appreciable changes in lightning. Finally, the plume rose to ~ 11 km before the end of ash emissions. It is intriguing that even though the maximum plume height (briefly) matched that of event 37 on March 8, the lightning rates never exceeded 4 strokes min^{-1} (compared to > 20 min^{-1} during

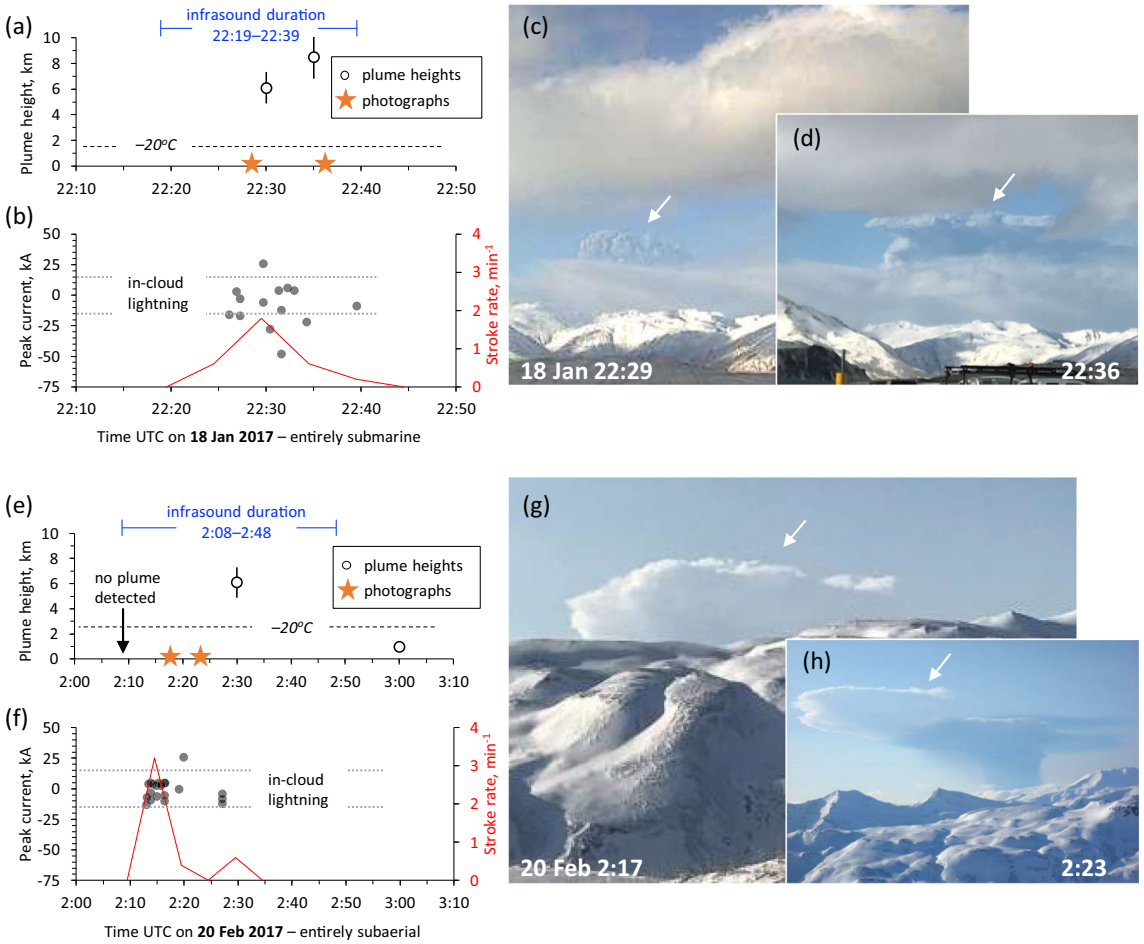

Fig. 9 Electrical activity, plume dynamics, and corresponding photos of two lower-intensity explosive events. Time-series data arranged as in Fig. 5, although infrasound spectrograms are not shown due to the shorter duration of activity. Stars give the timing of photographs included in the figure. **a–b** Data from the entirely subaerial explosion on 18 January 2016 (event 23). **c** Photograph taken at 22:29 UTC from the FAA webcam in Dutch Harbor, Alaska, ~98 km east of Bogoslof. **d** Photograph a few minutes later, at 22:36 UTC, taken by Victor Fisher in Dutch Harbor, when the plume reached ~8 km asl. **e–f** Data from the entirely submarine event 36 on 20 February. Photos of the 20 Feb plume were taken from the west side of Unalaska Island ~85 km ESE of Bogoslof volcano by Janet Schaefer at 2:17 UTC; AVO image ID 105941 in **g** and 2:23 UTC; AVO image ID 105151 in **h**. Note white arrows indicate the plume tops in each photo

event 37). This suggests that the *duration* of high-level emissions was an important factor—short-lived bursts do not seem to produce the same lightning abundance as sustained, higher-intensity eruptions (Smith 2019), as seen in Fig. 4b.

Two short-lived events—subaerial vs. submarine

From the observations described above, it seems that Bogoslof's lightning production was strongly modulated by plume rise into freezing levels of the atmosphere where ice charging could take place. A natural hypothesis is that increased magma-water interaction may lead to an increase in plume water and therefore an increase in ice-triggered lightning. Do the Bogoslof plumes from entirely underwater vents generate more lightning than their subaerial counterparts? It is only possible to address this question with Bogoslof's lower-intensity explosions, because none of the larger examples (with sustained plume heights > 10 km asl) were entirely subaerial. Here, we examine two short-duration, lower-level explosions (< 10 km asl) that sent ash above the freezing level during the Alaska winter, one entirely subaerial and one entirely submarine. Figure 9 shows that the events produced comparable amounts of lightning. Both had low stroke rates in the range of 1–4 min^{-1}, and only slight differences in the amount of higher-current (cloud-to-ocean) lightning.

Event 23 on 18 Jan occurred when Bogoslof's vent was above water (Fee et al. 2020). It produced a dark-gray cloud in visible satellite images, and a brightness temperature difference (Schneider et al. 2020). Although wind directions were not favorable for infrasound detection at the Okmok microphone array, satellite thermal data confirmed the presence of hot, fresh deposits on a subaerial vent following the explosion (Coombs et al. 2019). Photographs taken from Dutch Harbor

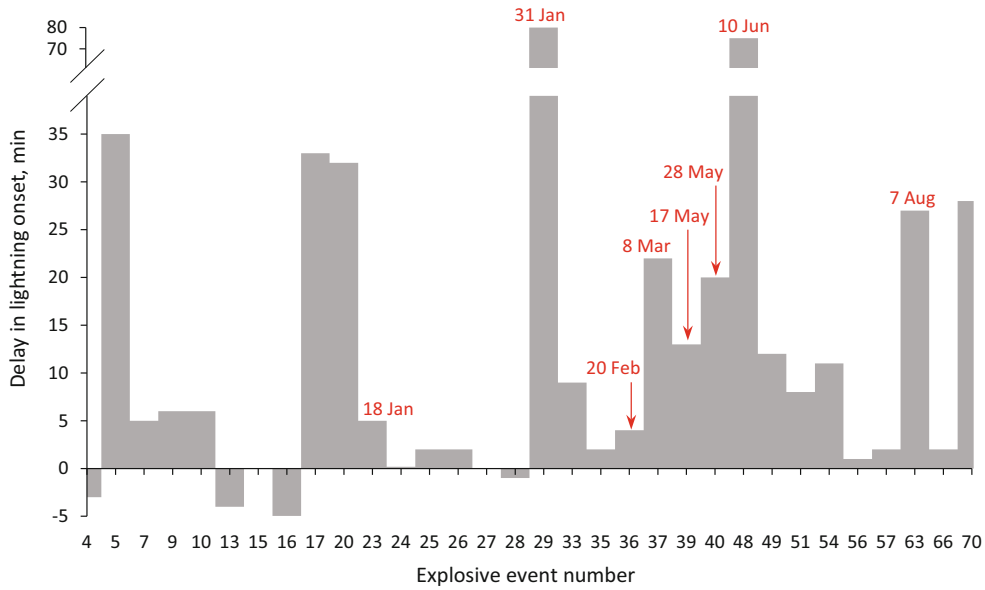

Fig. 10 Time delays from the start of eruptive behavior to the earliest onset of volcanic lightning. Plot only includes events with detectable lightning. Lightning onset was determined from the earliest detection from the following sources: the combined WWLLN and GLD360 dataset, two-sensor GLD360 solutions, or glitches from the Okmok infrasound array (Catalog B of Haney et al. 2020). The start of eruptive behavior was determined in post-analysis by the Alaska Volcano Observatory, relying heavily on infrasound (Coombs et al. 2019). Negative values indicate that lightning occurred before other geophysical signals. Lightning from event 56 (on 2 July) was detected by glitches only. Red labels show events examined in detail in this study. Note break in slope for events 29 (31 Jan) and 48 (10 June)

~98 km east (location in Fig. 1) show the plume's morphology during peak lightning generation (Fig. 9c, d).

Ash emissions lasted at least 16 min and produced scant, yet energetic lightning (peak 1.8 strokes min^{-1} with 43% of peak currents > 15 kA).

By comparison, the entirely submarine event 36 on 20 Feb produced similar lightning rates (3.2 strokes min^{-1}), although fewer were cloud-to-ocean strokes. Event 36 was categorized as submarine from the infrasound analysis of Fee et al. (2020), with daytime photographs of the plume development from Alaska Volcano Observatory scientists collecting ashfall on neighboring Unalaska Island (Fig. 9g, h). The explosion was short-lived and pulsatory, with a plume rising to 6.1 km asl by 2:30 UTC, and tapering off by 3:00. There was similar low-rate, low-current lightning during the submarine phase of event 29 on 31 Jan 2017 (Fig. 8a). Overall, the analysis shows no systematic difference between the lightning from submarine vs. subaerial episodes.

Discussion

Electrification processes during the Bogoslof eruption

Previous studies have demonstrated that silicate charging (unrelated to ice) can lead to visible, measurable lightning in small volcanic eruptions and laboratory-scale particle jets. Even the vaporization of seawater itself produces an electric charge in lab experiments (Björnsson et al. 1967; Pounder 1972). Thus, we were surprised to find that the Bogoslof eruption plumes only produced globally detectable lightning after they rose into the − 20 °C freezing level (Figs. 3, 5, 6, 7, 8, and 9). The overall pattern is consistent with observations from the 2010 eruption of Eyjafjallajökull in Iceland. Based on data from long-range detection systems, Arason et al. (2011) suggested a link between electrical activity and ice formation in the Eyjafjallajökull plumes. However, Behnke et al. (2014) observed much more lightning from that eruption using a close-range LMA system. They concluded that silicate charging was the dominant mechanism at Eyjafjallajökull because the vast majority of LMA-detected lightning initiated near the vent (Behnke et al. 2014), although ice formation may have had some influence (Woodhouse and Behnke 2014). From these studies, we infer that there was probably a sizeable population of Bogoslof's lightning that went undetected by our long-range methods. However, the undetected population must have been weak in this case, considering our ability to detect very low-current lightning (below 1–2 kA, keeping in mind the 25–50% uncertainty on those estimates). So did ice-charging influence Bogoslof's globally detected lightning or not?

On one hand, the lightning activity does not occur much farther than 25–30 km from Bogoslof (Fig. 1b) and does not persist long after the end of each eruptive event, generally shutting off within 10 min of the infrasound, if not sooner (Figs. 5, 7, and 8). This hints toward a (near-source) silicate

charging mechanism, which could be expected to stop when the eruption stops. On the other hand, several lines of evidence point to the influence of ice charging:

First, the ash plumes remained electrically quiet until they rose high enough to freeze (Figs. 5, 6, 7, 8, and 9). This is not the case at all volcanoes—for example, Sakurajima has generated high-current, globally-detectable lightning with plume heights < 3 km asl (Cassandra M. Smith, Unpublished Data). Yet, Bogoslof produced several plumes reaching > 3 km that failed to create lightning until freezing. Examples include a 40-min sequence of 3–5 km high plumes on 7 Aug (see Fig. 8d from 18:00–18:40 UTC; event 63) and the ~ 6.5 km plume on 28 May (see Fig. 5a at 22:30 UTC; event 40).

Second, analysis of stroke migration by Smith et al. (2018a) showed that lightning travel directions matched the trajectory of the upper-level ash cloud in 20 out of the 23 cases examined. This finding provides strong evidence that at least some of the globally detected lightning developed in situ within the upper cloud (c.f., Van Eaton et al. 2016), rather than initiating near the vent.

And third, thermodynamic modeling of Bogoslof's seawater-rich plumes, exemplified by event 40 on 28 March, points to a microphysical structure rivaling the most intense meteorological storms, with liquid water contents > 5 g m^{-3} and updrafts exceeding 40 m s^{-1} in the mixed-phase region (Fig. 6). Based on our modern understanding of severe weather, these conditions would undoubtedly lead to significant lightning triggered by ice-charging mechanisms (Saunders 2008; Emersic and Saunders 2010). In meteorological thunderstorms, collisional (noninductive) ice-charging drives the electrification process. Clouds become electrified when the following conditions are met: (1) strong updrafts 10–20 m s^{-1} extending several kilometers above the freezing level and (2) microphysical environments containing abundant supercooled liquid water, graupel, and small ice particles (Black and Hallett 1999; Reinhart et al. 2014). These ingredients create the conditions for electrifying collisions (Takahashi 1978; Saunders and Peck 1998; Saunders 2008; Emersic and Saunders 2010) and may explain why the explosions need to be sustained for several minutes well above the freezing level to produce abundant, globally detectable lightning. Shorter-lived pulses do not have time to generate the mixed-phase microphysical region and sustain a vertical flux through it. Recall the nine Bogoslof explosions that rose to the freezing level, but failed to produce lightning (Fig. 3c) due to their brief ash emissions (< 2 min, based on infrasound detection durations; Table 1). By virtue of their smaller area and ash loading in the atmosphere, these short-lived clouds were also unlikely to develop the extensive charge layers that lead to intense electrification (Behnke et al. 2013; Behnke and Bruning 2015).

If ice-charging matters, then the source of water is another issue. Why are not there more obvious differences between Bogoslof's subaerial eruptions and those blasting through seawater (Figs. 8 and 9)? Two potential explanations: (1) the observation may reflect limitations in our data, rather than a physical reality. We depended on low temporal- and spatial-resolution satellite data for the Bogoslof plume heights (rather than webcam or weather radar), and our long-range lightning data are limited compared to LMA. Therefore, it is possible that an electrical response to changing seawater input was simply below our detection capabilities. (2) Another possibility is that all of the explosive events were sufficiently water-rich to get the ice-charging process started. Perhaps most (if not all) of the explosions saw magma-water interaction with saturated sediments in the submarine conduit (Waythomas et al. 2020), and therefore contained abundant water in the plume. Our sensitivity study (Supplementary Fig. S1) shows that even a few percent external water could lead to appreciable supercooled liquid water contents in the upper plume (~ 0.5 g cm^{-3}). It is possible that all of the Bogoslof eruptions were *phreatomagmatic*, regardless of whether there was water present in the surficial crater. Satellite cloud observations certainly support this idea, with all but one explosion showing water-rich characteristics in multispectral imagery (Schneider et al. 2020); the Bogoslof plumes were demonstrably richer in water and ice than conventional 'dry' eruptions in Alaska, such as Pavlof 2016 (Fee et al. 2017).

Taken together, we infer that different charging mechanisms operated on continuum during the lifecycle of Bogoslof's eruption plumes. Silicate charging was probably active in the near-vent area during most of the explosions, producing weak electrical activity below our detection threshold, and perhaps even some of the lightning detected in this study. It was not until the plumes rose (and were sustained) above the freezing level, that ice-charging also came into play, triggering the observed, high rates of globally detectable lightning.

Volcanic lightning for monitoring

During the 9-month-long response effort, the Alaska Volcano Observatory used all available monitoring systems to detect and characterize Bogoslof's eruptive activity. No single method was foolproof on its own (Coombs et al. 2018, 2019). For example, infrasound signals were affected by local wind noise and complex propagation through the atmosphere (Schwaiger et al. 2020). Seismicity was complicated by ground motions coupling into the ocean, and interference with bathymetry of the ocean floor (Wech et al. 2018). Many of the satellite views were obscured by cloudy weather (Schneider et al. 2020). And lightning was detectable in fewer than half of the explosive events (this study). During this time, WWLLN provided a real-time

data feed of lightning within a 100 km radius of Bogoslof, which was used to program automated alerts (Coombs et al. 2018). The lightning provided a complementary tool to verify heightened activity at the volcano in context with seismoacoustic and satellite data. One explosion in particular (event 25 on 22 Jan) was raised to alert level red based on lightning alone (Coombs et al. 2018), because of challenges with seismic and infrasound detection. At the time, volcanic lightning added value in a purely qualitative sense—more strokes around the volcano probably meant more ash in the atmosphere. But detailed post-analysis from this study and other eruptions suggests some common traits among lightning-rich plumes. We explore two interrelated themes as working hypotheses for eruptions that create powerful, globally detectable lightning: (1) lightning indicates an ash-rich eruption and (2) it can take time for lightning to develop—indeed, some plumes may never produce detectable lightning at all.

(1) Lightning indicates an ash-rich eruption

This is a challenging hypothesis to test using historical data, because null results are rarely reported and detection methods vary wildly. But to our knowledge, there has not yet been an ash-free plume with volcanic lightning detected by long-range networks. The pioneering observations of Surtsey in Iceland from 1963 to 1967 showed that lightning only occurred in the presence of tephra jets, and was notably absent in the steam plumes, although those steam plumes did carry a net positive charge (Anderson et al. 1965). Likewise, the recent work of Nicoll et al. (2019) showed that ash-free gas plumes from Stromboli in Italy were charged, but failed to produce electrical breakdown in the form of lightning. Field studies at Sakurajima in Japan also emphasize that the more vigorous, ash-rich eruptions are associated with more lightning (Smith et al. 2018b; Smith 2019). In fact, the eruption of freshly fragmented, juvenile particles increased the likelihood of electrical activity compared to those dominated by older, lithic particles (Smith et al. 2018b). The simplest explanation is that without magma fragmentation, there is reduced fractoemission, and with fewer airborne particles, there are fewer opportunites for collisions followed by gravitational settling to separate and organize horizontal layers of charge. If volcanic lightning provides an indicator of airborne ash, then it provides a unique contribution to monitoring systems, because seismicity and infrasound can occur from numerous processes unrelated to ash emissions. Thus, globally detected lightning may help pinpoint the onset of ash-related hazards, as was the case at Calbuco in Chile (Van Eaton et al. 2016) and Kelud in Indonesia (Hargie et al. 2019). Yet, there are caveats, as discussed below.

(2) It takes time for plumes to develop globally-detected lightning (and some may not produce lightning at all). The Bogoslof eruption demonstrates how long it can take for plumes to become electrically active (Figs. 5, 6, 7, and 8). During the 2016–2017 eruption, plumes only became lightning-rich once they rose above the local freezing level, implying that mass eruption rates had to be sufficient to inject ash above −20 °C altitudes. Furthermore, several of the short-lived bursts (Fig. 3c) made it above the freezing level without ever generating detectable lightning. Figure 10 illustrates the delayed onset of volcanic lightning compared to the start of eruptive behavior determined for each explosion. Note, these start times are based on above-background geophysical signals, including infrasound and seismicity, which do not necessarily correspond to ash emissions (Coombs et al. 2019). There are considerable delays in some cases (events 29 and 48). Yet other times, lightning occurred earlier (events 4, 13, 16, and 28) or at about the same time as the recorded onset of eruptive activity (events 15, 24, and 27). The average offset is ~10 min, not counting the two outliers.

Event 48 on 10 June is an example of how lightning can dovetail nicely with other data streams. The infrasound signals ramped up ~4 h before any high-altitude ash emissions could be observed above the meteorological cloud deck ~6 km asl. There was also a gap in satellite coverage from 12:00 to 12:28 UTC, during which the plume began to rise into aircraft cruising levels (Fig. 8c). By using the onset of lightning in this instance (cable glitches at 11:15 and global lightning at 12:16), we could more clearly infer times when the ash plume rose above the freezing level. Another consideration is the propagation speed of lightning signals. Electromagnetic radiation travels at the speed of light (3×10^8 m/s), which is faster than seismic energy (solid earth waves; 3×10^3 m/s) and infrasound (air pressure waves; 3×10^2 m/s). This property leads to rapid alerts once the plume becomes electrically active—WWLLN's lightning alerts could typically arrive to AVO duty scientist phones within 1 or 2 min of lightning onset.

Conclusions

This study examines electrical activity during the eruption of Bogoslof, Alaska, using multiple ground-based methods of lightning detection from December 2016 to August 2017. In addition to lightning detected by global networks WWLLN and Vaisala's GLD360, we improved our sensitivity to small-

scale lightning by imposing a two-sensor solution on the GLD360 detections (making it possible to detect peak currents < 1 kA), and by also considering the electrical glitches from infrasound cables reported by Haney et al. (2020). We compared the lightning data with eruption column heights, atmospheric temperatures, and 1D plume modeling to explore the timing and mechanisms of plume electrification during the Surtseyan eruptive activity. Our analysis reveals the following:

- Globally detected lightning only occurred during sustained injection of volcanic plumes above the local atmospheric freezing level (approximated by the − 20 °C isotherm as in Arason et al. (2011)).
- The plumes remained electrically quiet until they rose high enough to freeze, even at heights of 3–5 km asl for more than 30 min (e.g., event 63 on 7 Aug; Fig. 8d).
- Lightning activity was not focused only in the low-altitude regions of the plumes, as would be expected in a system dominated by silicate charging (Behnke et al. 2014). Rather, it followed the ash clouds downwind through time (Smith et al. 2018a), indicating in situ charging within the upper plumes
- 1D modeling of the water-rich plumes suggests liquid water contents > 5 g m^{-3} and updrafts exceeding 40 m s^{-1} in the mixed-phase region—ideal conditions for vigorous ice charging (Fig. 6)
- We infer that ice charging was a catalyst of globally detectable lightning for these small to moderate-intensity events (mass eruption rates in the range of 10^4–10^6 kg s^{-1}). However, it is likely that silicate-charging was also at play, contributing to the overall charge evolution and generating weak, near-vent electrical activity that was below the sensitivity of our instruments
- More than half of the 70 explosions failed to become electrically active, including several short-lived bursts that rose to − 20 °C altitudes without producing lightning. We infer that these ash plumes were not sustained long enough to buildup sufficient charge. Sustained ash emissions > 5 min increased the likelihood of globally detectable lightning (Fig. 4b).
- The presence of seawater in the vent did not systematically affect lightning generation within uncertainty of our measurements, except perhaps in the case of 31 Jan 2017 (event 29). The Bogoslof plumes may have carried sufficient water for ice-charging regardless of whether they erupted through water or directly into air during the final stage of ascent. It is possible that rising magma incorporated external water from submarine strata during most, if not all, of the events.
- Improving our ability to detect weak, low-current lightning was important for early identification of ash emissions, because the vast majority of Bogoslof's volcanic lightning was in-cloud (peak currents less than ± 15 kA), rather than cloud-to-ocean.
- A strength of volcanic lightning detection within the broader suite of monitoring tools is verification of airborne ash, because lightning is rare or perhaps absent in ash-free plumes of steam. The electrification process may take some time to develop (minutes to tens of minutes), depending on plume height relative to the atmospheric freezing level. During the Bogoslof eruption, globally detected volcanic lightning provided a reliable indication of sustained, ash-rich plumes reaching (or exceeding) the local − 20 °C freezing altitude.
- In eruption plumes that rise high enough to freeze, electrical charging mechanisms may operate on a continuum—with silicate charging dominant in the near-vent region, and collisional ice charging taking place in the higher-level plumes during growth of mixed-phase hydrometeors.

Acknowledgments We wish to thank the World Wide Lightning Location Network (http://wwlln.net), a collaboration among over 50 universities and institutions, for providing WWLLN lightning location data. We also thank Vaisala, Inc. for providing the GLD360 data used in this study. Michael Pavolonis (NOAA/NESDIS) is acknowledged for plume height retrievals using Himawari-8. Two anonymous reviewers are thanked for their thorough comments, which greatly improved the manuscript. Any use of trade, firm, or product names is for descriptive purposes only and does not imply endorsement by the U.S. Government. Data used in this study are provided in the references, tables, and Supplementary Material.

Funding information Funding for the study was provided by the USGS Volcano Hazards Program. RHH also received funding from NASA grant 80NSSC19K0407.

References

Abarca SF, Corbosiero KL, Galarneau TJ (2010) An evaluation of the worldwide lightning location network (WWLLN) using the National Lightning Detection Network (NLDN) as ground truth. J Geophys Res 115:D18206. https://doi.org/10.1029/2009jd013411

Anderson R, Björnsson S, Blanchard DC, Gathman S, Hughes J, Jónasson S, Moore CB, Survilas HJ, Vonnegut B (1965) Electricity in volcanic clouds. Science 148:1179–1189 https://www.jstor.org/stable/1716180

Andrews VP, Genareau KD, Naeger A, Schulz CJ (2018) Using NASA and NOAA satellite data to improve volcanic ash plume modeling for impact-based decision support. Abstract A41G-3044 presented at fall AGU meeting, Washington, D.C, 10–14 Dec. https://agu.confex.com/agu/fm18/meetingapp.cgi/Paper/467280

Arason P, Bennett AJ, Burgin LE (2011) Charge mechanism of volcanic lightning revealed during the 2010 eruption of Eyjafjallajökull. J Geophys Res 116:B00C03. https://doi.org/10.1029/2011jb008651

Behnke SA, Bruning EC (2015) Changes to the turbulent kinematics of a volcanic plume inferred from lightning data. Geophys Res Lett 42: 4232–4239. https://doi.org/10.1002/2015gl064199

Behnke SA, McNutt SR (2014) Using lightning observations as a volcanic eruption monitoring tool. Bull Volcanol 76:847–812. https://doi.org/10.1007/s00445-014-0847-1

Behnke SA, Thomas RJ, McNutt SR, Schneider DJ, Krehbiel PR, Rison W, Edens HE (2013) Observations of volcanic lightning during the 2009 eruption of redoubt volcano. J Volcanol Geotherm Res 259: 214–234. https://doi.org/10.1016/j.jvolgeores.2011.12.010

Behnke SA, Thomas RJ, Edens HE, Krehbiel PR, Rison W (2014) The 2010 eruption of Eyjafjallajökull: lightning and plume charge structure. J Geophys Res 119:833–859. https://doi.org/10.1002/2013jd020781

Behnke SA, Edens HE, Thomas RJ, Smith CM, McNutt SR, Van Eaton AR, Cimarelli C, Cigala V (2018) Investigating the origin of continual radio frequency impulses during explosive volcanic eruptions. J Geophys Res Atmos 123:4157–4174. https://doi.org/10.1002/2017jd027990

Biagi CJ, Cummins KL, Kehoe KE, Krider EP (2007) National Lightning Detection Network (NLDN) performance in southern Arizona, Texas, and Oklahoma in 2003–2004. J Geophys Res 112:D05208. https://doi.org/10.1029/2006jd007341

Bitzer PM, Burchfield JC (2016) Bayesian techniques to analyze and merge lightning locating system data. Geophys Res Lett 43:12, 605–612,613. https://doi.org/10.1002/2016gl071951

Björnsson S, Blanchard DC, Spencer AT (1967) Charge generation due to contact of saline waters with molten lava. J Geophys Res 72:1311–1323

Black RA and Hallett J (1999): Electrification of the Hurricane. J. Atmos. Sci., 56:2004–2028. https://doi.org/10.1175/1520-0469(1999)056<2004:EOTH>2.0.CO;2

Cimarelli C, Alatorre-Ibarguengoitia MA, Kueppers U, Scheu B, Dingwell DB (2013) Experimental generation of volcanic lightning. Geology 42:79–82. https://doi.org/10.1130/g34802.1

Cimarelli C, Alatorre-Ibargüengoitia MA, Aizawa K, Yokoo A, Díaz-Marina A, Iguchi M, Dingwell DB (2016) Multiparametric observation of volcanic lightning: Sakurajima volcano, Japan. Geophys Res Lett 43:4221–4228. https://doi.org/10.1002/2015gl067445

Coombs ML, Wech AG, Haney MM, Lyons JJ, Schneider DJ, Schwaiger HF, Wallace KL, Fee D, Freymueller JT, Schaefer JR, Tepp G (2018) Short-term forecasting and detection of explosions during the 2016–2017 eruption of Bogoslof volcano, Alaska. Front Earth Sci 6. https://doi.org/10.3389/feart.2018.00122

Coombs M, Wallace K, Cameron C, Lyons J, Wech A, Angeli K, Cervelli P (2019) Overview, chronology, and impacts of the 2016–2017 eruption of Bogoslof volcano, Alaska. Bull Volcanol 81:62. https://doi.org/10.1007/s00445-019-1322-9

Deierling W, Petersen WA, Latham J, Ellis S, Christian HJ (2008) The relationship between lightning activity and ice fluxes in thunderstorms. J Geophys Res 113:D15210. https://doi.org/10.1029/2007jd009700

Emersic C, Saunders CPR (2010) Further laboratory investigations into the relative diffusional growth rate theory of thunderstorm electrification. Atmos Res 98:327–340. https://doi.org/10.1016/j.atmosres.2010.07.011

Fee D, Haney MM, Matoza RS, Van Eaton AR, Cervelli P, Schneider DJ, Iezzi AM (2017) Volcanic tremor and plume height hysteresis from Pavlof volcano, Alaska. Science 355:45–48

Fee D, Lyons J, Haney M, Wech A, Waythomas C, Diefenbach AK, Lopez T, Van Eaton AR, Schneider D (2020) Seismo-acoustic evidence for vent drying during shallow submarine eruptions at Bogolsof volcano, Alaska. Bull Volcanol 82:2. https://doi.org/10.1007/s00445-019-1326-5

Garrett TJ, Dean-Day J, Liu C, Barnett B, Mace G, Baumgardner D, Webster C, Bui T, Read W, Minnis P (2006) Convective formation of pileus cloud near the tropopause. Atmos Chem Phys 6:1185–1200 www.atmos-chem-phys.net/6/1185/2006/

Gaudin D, Cimarelli C (2019) The electrification of volcanic jets and controlling parameters: a laboratory study. Earth Planet Sci Lett 513:69–80. https://doi.org/10.1016/j.epsl.2019.02.024

Haney MM, Van Eaton AR, Lyons JJ, Kramer RL, Fee D, Iezzi AM (2018) Volcanic thunder from explosive eruptions at Bogoslof volcano, Alaska. Geophys Res Lett 45:3429–3435. https://doi.org/10.1002/2017gl076911

Haney MM, Van Eaton AR, Lyons JJ, Kramer RL, Fee D, Iezzi AM, Dziak RP, Anderson J, Johnson JB, Lapierre JL, Stock M (2020) Characteristics of thunder and electromagnetic pulses from volcanic lightning at Bogoslof volcano, Alaska. Bull Volcanol 82:15. https://doi.org/10.1007/s00445-019-1349-y

Hargie KA, Van Eaton AR, Mastin LG, Holzworth RH, Ewert JW, Pavolonis M (2019) Globally detected volcanic lightning and umbrella dynamics during the 2014 eruption of Kelud, Indonesia. J Volcanol Geotherm Res 382:81–91. https://doi.org/10.1016/j.jvolgeores.2018.10.016

Houghton B, White JDL, Van Eaton AR (2015) Phreatomagmatic and related eruption styles. In: Sigurdsson H, Houghton BF, Rymer H, Stix J, McNutt SR (eds) The encyclopedia of volcanoes. Academic Press, San Diego, pp 537–552

Hutchins ML, Holzworth RH, Brundell JB, Rodger CJ (2012a) Relative detection efficiency of the world wide lightning location network. Radio Sci 47:RS6005. https://doi.org/10.1029/2012rs005049

Hutchins ML, Holzworth RH, Rodger CJ, Heckman S, Brundell JB (2012b) WWLLN absolute detection efficiencies and the global lightning source function. Geophys Res Abstr 14:EGU2012–EG12917

James MR, Lane SJ, Gilbert JS (2000) Volcanic plume electrification: experimental investigation of a fracture-charging mechanism. J Geophys Res Solid Earth 105:16641–16649. https://doi.org/10.1029/2000jb900068

James MR, Wilson L, Lane SJ, Gilbert JS, Mather TA, Harrison RG, Martin RS (2008) Electrical charging of volcanic plumes. Space Sci Rev 137:399–418. https://doi.org/10.1007/s11214-008-9362-z

Jónasson S (1965) Cover photo: Lightning in volcano cloud. Science 148(3674) https://science.sciencemag.org/content/sci/148/3674/local/front-matter.pdf

Lapierre J, Van Eaton AR, Stock M, Haney MM, Lyons JJ (2018) Remote measurements of volcanic plume electrification using a sparse network technique. Abstract O2–11 presented at the WMO technical conference on meteorological and environmental Instrumenets and methods of observation Amsterdam, the Netherlands 8–11 October 2018. https://www.wmocimo.net/wp-content/uploads/O2_11_Lapierre_2018_cimo-teco_extended_abstract_final.pdf

LaRoche KT, Lang TJ (2017) Observations of ash, ice, and lightning within pyrocumulus clouds using polarimetric NEXRAD radars and the National Lightning Detection Network. Mon Weather Rev 145:4899–4910. https://doi.org/10.1175/mwr-d-17-0253.1

Loewen MW, Izbekov P, Moshrefzadeh J, Coombs M, Larsen J, Graham N, Harbin M, Waythomas C, Wallace K (2019) Petrology of the 2016–2017 eruption of Bogoslof Island, Alaska. Bull Volcanol 81:72. https://doi.org/10.1007/s00445-019-1333-6

Loney ML, Zrnić DS, Straka JM, Ryzhkov AV (2002) Enhanced polarimetric radar signatures above the melting level in a supercell storm. J Appl Meteorol 41:1179–1194

Lopez T, Clarisse L, Schwaiger HF, Van Eaton AR, Loewen MW, Fee D, Lyons JJ, Wallace KL, Searcy C, Wech AG, Schneider DJ, Haney MM, Graham N (2020) Constraints on eruption processes and event masses for the 2016-2017 eruption of Bogoslof volcano, Alaska, through evaluation of IASI satellite SO2 masses and complementary datasets. Bull Volcanol (part of the Bogoslof Topical Collection). https://doi.org/10.1007/s00445-019-1348-z

Lyons JJ, Haney MM, Fee D, Wech A, Waythomas C (2019) Infrasound from giant bubbles during explosive submarine eruptions of Bogoslof volcano, Alaska. Nat Geosci 12:952–958. https://doi.org/10.1038/s41561-019-0461-0

Lyons JJ, Iezzi AM, Fee D, Schwaiger HF, Wech AG, Haney MM (2020) Infrasound generated by the 2016-17 shallow submarine eruption of

Bogoslof volcano, Alaska. Bull Volcanol (part of the Bogoslof Topical Collection). https://doi.org/10.1007/s00445-019-1355-0

Mallick S, Rakov VA, Ngin T, Gamerota WR, Pilkey JT, Hill JD, Uman MA, Jordan DM, Nag A, Said RK (2014) Evaluation of the GLD360 performance characteristics using rocket-and-wire triggered lightning data. Geophys Res Lett 41:3636–3642. https://doi.org/10.1002/2014gl059920

Mastin LG (2007) A user-friendly one-dimensional model for wet volcanic plumes. Geochem Geophys Geosyst 8:Q03014. https://doi.org/10.1029/2006GC001455

Mastin LG (2014) Testing the accuracy of a 1-D volcanic plume model in estimating mass eruption rate. J Geophys Res 119:2474–2495. https://doi.org/10.1002/2013JD020604

Mastin LG, Guffanti M, Servranckx R, Webley P, Barsotti S, Dean K, Durant A, Ewert JW, Neri A, Rose WI, Schneider D, Siebert L, Stunder B, Swanson G, Tupper A, Volentik A, Waythomas CF (2009) A multidisciplinary effort to assign realistic source parameters to models of volcanic ash-cloud transport and dispersion during eruptions. J Volcanol Geotherm Res 186:10–21. https://doi.org/10.1016/j.jvolgeores.2009.01.008

Mather TA, Harrison RG (2006) Electrification of volcanic plumes. Surv Geophys 27:387–432. https://doi.org/10.1007/s10712-006-9007-2

McNutt SR, Williams ER (2010) Volcanic lightning: global observations and constraints on source mechanisms. Bull Volcanol 72:1153–1167. https://doi.org/10.1007/s00445-010-0393-4

Méndez Harper J, Dufek J (2016) The effects of dynamics on the triboelectrification of volcanic ash. J Geophys Res Atmos 121:8209–8228. https://doi.org/10.1002/2015jd024275

Moore JG (1985) Structure and eruptive mechanisms at Surtsey volcano, Iceland. Geol Mag 122:649–661. https://doi.org/10.1017/S0016756800032052

Moxnes ED, Kristiansen NI, Stohl A, Clarisse L, Durant A, Weber K, Vogel A (2014) Separation of ash and sulfur dioxide during the 2011 Grímsvötn eruption. J Geophys Res Atmos 119:7477–7501. https://doi.org/10.1002/2013JD021129

Nicoll K, Airey M, Cimarelli C, Bennett A, Harrison G, Gaudin D, Aplin K, Koh KL, Knuever M, Marlton G (2019) First In Situ Observations of Gaseous Volcanic Plume Electrification. Geophys. Res. Lett. 46(6):3532–3539. https://doi.org/10.1029/2019gl082211

Pessi AT, Businger S, Cummins KL, Demetriades NWS, Murphy M, Pifer B (2009) Development of a long-range lightning detection network for the Pacific: construction, calibration, and performance. J Atmos Ocean Technol 26:145–166. https://doi.org/10.1175/2008jtecha1132.1

Pounder C (1972) Electrification from salt water on heated metals. J Phys D Appl Phys 5:753–755. https://doi.org/10.1088/0022-3727/5/4/415

Reinhart B, Fuelberg H, Blakeslee R, Mach D, Heymsfield A, Bansemer A, Durden SL, Tanelli S, Heymsfield G, Lambrigtsen B (2014) Understanding the relationships between lightning, cloud microphysics, and airborne radar-derived storm structure during Hurricane Karl (2010). Monthly Weather Review 142(2):590–605. https://doi.org/10.1175/mwr-d-13-00008.1

Rodger CJ, Brundell JB, Dowden RL (2005) Location accuracy of VLF world-wide lightning location (WWLL) network: post-algorithm upgrade. Ann Geophys 23:277–290. https://doi.org/10.5194/angeo-23-277-2005

Rybin A, Chibisova M, Webley P, Steensen T, Izbekov P, Neal C, Realmuto V (2011) Satellite and ground observations of the June 2009 eruption of Sarychev peak volcano, Matua Island, central Kuriles. Bull Volcanol 73:1377–1392. https://doi.org/10.1007/s00445-011-0481-0

Said R (2018) Analysis of VLF Sferic attenuation in the earth-ionosphere waveguide using GLD360 sensor data. Abstract AE21B-3133 presented at fall AGU meeting, Washington, D.C.

Said R, Murphy M (2016) GLD360 upgrade: performance analysis and applications. Presented at the 24th international lightning detection conference & 6th international lightning meteorology conference. https://www.vaisala.com/sites/default/files/documents/Ryan%20Said%20and%20Martin%20Murphy.%20GLD360%20Upgrade%20Performance%20Analysis%20and%20Applications.pdf

Said RK, Inan US, Cummins KL (2010) Long-range lightning geolocation using a VLF radio atmospheric waveform bank. J Geophys Res 115. https://doi.org/10.1029/2010jd013863

Said RK, Cohen MB, Inan US (2013) Highly intense lightning over the oceans: estimated peak currents from global GLD360 observations. J Geophys Res Atmos 118:6905–6915. https://doi.org/10.1002/jgrd.50508

Saunders C (2008) Charge separation mechanisms in clouds. Space Sci Rev 137:335–353. https://doi.org/10.1007/s11214-008-9345-0

Saunders CPR, Peck SL (1998) Laboratory studies of the influence of the rime accretion rate on charge transfer during crystal/graupel collisions. J Geophys Res Atmos 103:13949–13956. https://doi.org/10.1029/97jd02644

Schill GP, Genareau K, Tolbert MA (2015) Deposition and immersion-mode nucleation of ice by three distinct samples of volcanic ash. Atmos Chem Phys 15:7523–7536. https://doi.org/10.5194/acp-15-7523-2015

Schipper CI, White JDL (2016) Magma-slurry interaction in Surtseyan eruptions. Geology 44:195–198. https://doi.org/10.1130/g37480.1

Schneider DJ, Rose WI, Coke LR, Bluth GJS (1999) Early evolution of a stratospheric volcanic eruption cloud as observed with TOMS and AVHRR. J Geophys Res 104:4037–4050

Schneider DJ, Van Eaton AR, Wallace KL (2020) Satellite observations of the 2016-17 Eruption of Bogoslof volcano: aviation and ash fallout hazard implications from a water-rich eruption. Bull Volcanol (part of the Bogoslof Topical Collection)

Schultz EV, Schultz CJ, Carey LD, Cecil DJ, Bateman M (2016) Automated Storm Tracking and the Lightning Jump Algorithm Using GOES-R Geostationary Lightning Mapper (GLM) Proxy Data. J Operat Meteorol 4:92–107. https://doi.org/10.15191/nwajom.2016.0407

Schwaiger HF, Lyons JJ, Iezzi AM, Haney M (2020) Evolving infrasound detections from Bogoslof volcano, Alaska: Insights from atmospheric propagation modeling. Bull Volcanol (part of the Bogoslof Topical Collection)

Shevtsov BM, Firstov PP, Cherneva NV, Holzworth RH, Akbashev RR (2016) Lightning and electrical activity during the Shiveluch volcano eruption on 16 November 2014. Nat Hazards Earth Syst Sci 16:871–874. https://doi.org/10.5194/nhess-16-871-2016

Smith CM (2019) Volcanic Electrification: A multiparametric case study of Sakurajima Volcano, Japan. PhD Thesis, University of South Florida

Smith CM, Van Eaton AR, Said R, Holzworth RH (2018a) Volcanic lightning as a monitoring tool during the 2016–2017 eruption of Bogoslof volcano, AK. Abstract presented at the International Lightning Detection Conference/ International Lightning Meteorology Conference, 12–15 March, Ft. Lauderdale. https://www.vaisala.com/sites/default/files/documents/Volcanic%20lightning%20as%20monitoring%20tool%20during%202016-2017%20eruption%20of%20Bogoslof%20Volcano%20AK_C.M.%20Smith%20et%20al.pdf

Smith CM, Van Eaton AR, Charbonnier S, McNutt SR, Behnke SA, Thomas RJ, Edens HE, Thompson G (2018b) Correlating the electrification of volcanic plumes with ashfall textures at Sakurajima volcano, Japan. Earth Planet Sci Lett 492:47–58. https://doi.org/10.1016/j.epsl.2018.03.052

Takahashi T (1978) Riming electrification as a charge generation mechanism in thunderstorms. J. Atmos. Sci. 35:1536–1548. https://doi.org/10.1175/1520-0469(1978)035<1536:REAACG>2.0.CO;2

Tepp G, Dziak RP, Haney MM, Lyons JJ, Searcy C, Matsumoto H, Haxel J (2020) Seismic and hydroacoustic observations of the 2016-17 Bogoslof eruption. Bull Volcanol 82:4. https://doi.org/10.1007/s00445-019-1344-3

Thomas RJ, McNutt SR, Krehbiel PR, Rison W, Aulich G, Edens HE, Tytgat G, Clark E (2010) Lightning and electrical activity during the 2006 eruption of Augustine volcano. US Geol Surv Prof Pap 1769: 579–608

Thorarinsson S (1967) Surtsey—the New Island in the North Atlantic. Viking Press, New York, p 105

Tsutomu T (1978) Riming electrification as a charge generation mechanism in thunderstorms. J Atmos Sci 35:1536–1548. https://doi.org/10.1175/1520-0469(1978)035<1536:REAACG>2.0.CO;2

Van Eaton AR, Herzog M, Wilson CJN, McGregor J (2012) Ascent dynamics of large phreatomagmatic eruption clouds: the role of microphysics. J Geophys Res 117:B03203. https://doi.org/10.1029/2011JB008892

Van Eaton AR, Mastin LG, Herzog M, Schwaiger HF, Schneider DJ, Wallace KL, Clarke AB (2015) Hail formation triggers rapid ash aggregation in volcanic plumes. Nat Commun 6:7860. https://doi.org/10.1038/ncomms8860

Van Eaton AR, Amigo Á, Bertin D, Mastin LG, Giacosa RE, González J, Valderrama O, Fontijn K, Behnke SA (2016) Volcanic lightning and plume behavior reveal evolving hazards during the April 2015 eruption of Calbuco volcano, Chile. Geophys Res Lett 43:3563–3571. https://doi.org/10.1002/2016GL068076

Walker G, Croasdale R (1972) Characteristics of some basaltic pyroclasts. Bull Volcanol 35:303–317. https://doi.org/10.1007/BF02596957

Waythomas CF, Angeli K, Wessels RL (2020) Evolution of the submarine-subaerial edifice of Bogoslof volcano, Alaska, during its 2016-2017 eruption based on analysis of satellite imagery. Bull Volcanol (part of the Bogoslof Topical Collection)

Wech A, Tepp G, Lyons J, Haney M (2018) Using earthquakes, T waves, and infrasound to investigate the eruption of Bogoslof volcano, Alaska. Geophys Res Lett 45:6918–6925. https://doi.org/10.1029/2018gl078457

Williams ER (1995) Comment on "thunderstorm electrification laboratory experiments and charging mechanisms" by C.P.R. Saunders. J Geophys Res 100:1503–1505

Williams ER, McNutt SR (2005) Total water contents in volcanic eruption clouds and implications for electrification and lightning. In: Pontikis C (ed) Recent Progress in lightning physics. Research signpost, Thiruvananthapuram, Trivandrum pp 81–94

Williams E, Nathou N, Hicks E, Pontikis C, Russell B, Miller M, Bartholomew MJ (2009) The electrification of dust-lofting gust fronts ('haboobs') in the Sahel. Atmos Res 91:292–298. https://doi.org/10.1016/j.atmosres.2008.05.017

Woodhouse MJ, Behnke SA (2014) Charge structure in volcanic plumes: a comparison of plume properties predicted by an integral plume model to observations of volcanic lightning during the 2010 eruption of Eyjafjallajökull, Iceland. Bull Volcanol 76:1–21. https://doi.org/10.1007/s00445-014-0828-4